JOURNAL OF PETROLOGY | VOLUME 48 | NUMBER 9 | PAGES 1813–1840 | 2007 | doi:10.1093/petrology/egm040

Geochemistry of Cretaceous Magmatism in Eastern Cuba: Recycling of North American Continental Sediments and Implications for Subduction Polarity in the Greater Antilles Paleo-arc

CLAUDIO MARCHESI[1,2]*, CARLOS J. GARRIDO[1,2], DELPHINE BOSCH[3], JOAQUÍN A. PROENZA[4], FERNANDO GERVILLA[1,2], PATRICK MONIÉ[5] AND ANTONIO RODRÍGUEZ-VEGA[6]

[1]DEPARTAMENTO DE MINERALOGÍA Y PETROLOGÍA, FACULTAD DE CIENCIAS, UNIVERSIDAD DE GRANADA, 18002 GRANADA, SPAIN

[2]INSTITUTO ANDALUZ DE CIENCIAS DE LA TIERRA, FACULTAD DE CIENCIAS, UNIVERSIDAD DE GRANADA-CSIC, 18002 GRANADA, SPAIN

[3]GÉOSCIENCES MONTPELLIER, ÉQUIPE MANTEAU-NOYAU, UMR 5243, CNRS-UNIVERSITÉ MONTPELLIER II, 34095 MONTPELLIER, FRANCE

[4]DEPARTAMENT DE CRISTAL·LOGRAFIA, MINERALOGIA I DIPÒSITS MINERALS, FACULTAT DE GEOLOGIA, UNIVERSITAT DE BARCELONA, 08028 BARCELONA, SPAIN

[5]GÉOSCIENCES MONTPELLIER, ÉQUIPE LITHOSPHÈRE, UMR 5243, CNRS-UNIVERSITÉ MONTPELLIER II, 34095 MONTPELLIER, FRANCE

[6]DEPARTAMENTO DE GEOLOGÍA, INSTITUTO SUPERIOR MINERO-METALÚRGICO, 83320 MOA, HOLGUÍN, CUBA

RECEIVED SEPTEMBER 21, 2006; ACCEPTED JUNE 29, 2007

We present whole-rock major- and trace-element and Nd–Sr–Pb radiogenic isotope data for Cretaceous igneous suites from eastern Cuba. These rocks are related to the Greater Antilles paleo-island arc magmatism and have three different igneous styles. Group 1 consists of tholeiitic basalts and rare basaltic andesites that have normal mid-ocean ridge basalt (N-MORB)-like compositions similar to those found in back-arc basin basalts ($TiO_2 = 1{\cdot}2–2{\cdot}9$ wt%; $La/Yb_{(N)} = 0{\cdot}7–0{\cdot}9$, $Th/Nb = 0{\cdot}06–0{\cdot}08$, and initial $^{208}Pb/^{204}Pb = 37{\cdot}65–37{\cdot}74$). Group 2 comprises basaltic and rare basaltic andesitic subvolcanic dykes with major- and trace-element and isotopic compositions similar to those of island arc tholeiites ($TiO_2 = 0{\cdot}7–1{\cdot}4$ wt%; $La/Yb_{(N)} = 0{\cdot}6–0{\cdot}9$, $Th/Nb = 0{\cdot}06–0{\cdot}68$, and initial $^{208}Pb/^{204}Pb = 37{\cdot}74–38{\cdot}25$). Group 3 is composed of low-Ti ($TiO_2 = 0{\cdot}3–0{\cdot}9$ wt%) calcalkaline igneous rocks that have an unambiguous subduction-related character ($La/Yb_{(N)} = 1{\cdot}1–5{\cdot}0$, $Th/Nb = 0{\cdot}35–1{\cdot}55$, and initial $^{208}Pb/^{204}Pb = 37{\cdot}94–38{\cdot}39$). The parental magmas of the three groups formed by variable melting degrees (<5–25%) of spinel lherzolite, with more depleted mantle sources for Groups 2 and 3 than Group 1. The trace-element and radiogenic isotope compositions of primitive Group 3 samples are strongly bimodal. One subgroup of samples is characterized by low Ta/Yb (0·02–0·03) and Th/La (0·10–0·13), slightly subchondritic Nb/Ta (13·3–17·3), and relatively high initial $^{206}Pb/^{204}Pb$ (18·57–18·62) and ϵ_{Nd} (7·6–9·4). The remaining primitive Group 3 samples have higher Ta/Yb (0·06–0·11) and Th/La (0·24–0·32), and highly subchondritic

*Corresponding author. Present address: Departamento de Mineralogía y Petrología, Facultad de Ciencias, Avenida Fuentenueva s/n, 18002 Granada, Spain. Telephone: + 34 958 248535. Fax: +34 958 243368. E-mail: claudio@ugr.es

Nb/Ta (7·6–9·1), coupled with lower initial $^{206}Pb/^{204}Pb$ (18·24–18·29) and ϵ_{Nd} (3·4–5·5). These signatures were induced by two distinct slab components that mainly reflect the contributions of Cretaceous Atlantic marine and North American continental sediments, respectively. Nb/Ta in the first subgroup was influenced by melting of rutile-bearing subducted crust, whereas in the second it was inherited from recycled continental sediments. The involvement of Atlantic and North American sediments in Cuban Cretaceous magmatism indicates that the Proto-Caribbean (North American-Proto Atlantic) lithosphere subducted beneath the Greater Antilles arc during the Late Cretaceous (pre-Campanian), consistent with geotectonic models involving onset of SW-dipping subduction beneath the Greater Antilles paleo-arc during the Aptian. The variable mantle source depletion and magnitude of the subduction component probably reflect different settings across the arc, from the arc front to a back-arc spreading ridge.

KEY WORDS: *eastern Cuba; Greater Antilles paleo-island arc; mantle source depletion; Nb/Ta fractionation; slab component*

INTRODUCTION

The Greater Antilles paleo-island arc, consisting of Cuba, Jamaica, Hispaniola, Puerto Rico and the Virgin Islands, marked the Cretaceous plate boundary between the Caribbean and North American plates. One point of recurring controversy in models of Caribbean tectonic evolution is the polarity of subduction beneath this extinct island arc system during the Late Cretaceous (Kerr *et al.*, 1999, 2003; Jolly *et al.*, 2001; Pindell *et al.*, 2006). The two main alternatives proposed in the literature are the SW-dipping subduction of Proto-Caribbean (North American-Proto Atlantic) oceanic lithosphere beneath the Caribbean plate and an opposite NE-dipping geometry. Insight into the polarity and evolution of the Greater Antilles paleo-arc system can be obtained through consideration of the mantle and slab components involved in the genesis of the Caribbean arc-related igneous rocks.

Here we present new whole-rock major- and trace-element and Nd–Sr–Pb radiogenic isotope data for Cretaceous igneous suites from eastern Cuba. Our study complements recent geochemical investigations of igneous suites in other parts of the Mesozoic Greater Antilles arc system (Jolly *et al.*, 2001, 2006; Escuder Viruete *et al.*, 2006). We exploit variations of middle rare earth elements (MREE), heavy REE (HREE), high field strength elements (HFSE) and Pb radiogenic isotope ratios of Cuban primitive basalts to (1) evaluate the composition and the degree of melting of the mantle source and (2) assess and identify the nature of the slab component involved in their genesis. These geochemical data are used to reconstruct the tectonic setting of the Cretaceous magmatism in eastern Cuba and to constrain the subduction polarity of the Greater Antilles paleo-island arc during the Mesozoic. Furthermore, we show how Nb–Ta abundances in primitive Cuban arc rocks, which are considered either unaffected by slab contributions (Pearce, 1983; McCulloch & Gamble, 1991; Pearce & Parkinson, 1993; Woodhead *et al.*, 1993) or significantly transferred from the subducting lithosphere to the mantle wedge by slab melts (Stolz *et al.*, 1996; Münker, 1998; Prouteau *et al.*, 2000; Foley *et al.*, 2002; Münker *et al.*, 2004; Gómez-Tuena *et al.*, 2007), were influenced by different slab components related to the SW-dipping subduction of the Proto-Caribbean plate beneath the Greater Antilles paleo-arc.

GEOLOGICAL SETTING

The tectonics of the modern Caribbean has been shaped primarily by two main geodynamic events: first, the breakup of North America and Gondwana led to the opening of the Proto-Caribbean oceanic basin; this stage was followed by a collisional event linked to the convergence of the Proto-Caribbean (North American-Proto Atlantic) and Caribbean plates (e.g. Lewis & Draper, 1990; Pindell, 1994; Iturralde-Vinent, 1998; Meschede & Frisch, 1998, and references therein). During the latter stage, the extinct Greater Antilles Island Arc formed, which now comprises parts of Cuba, Jamaica, Hispaniola, Puerto Rico and the Virgin Islands.

Three major igneous suites are commonly recognized in the volcanic and plutonic record of the modern Caribbean (Donnelly & Rogers, 1980; Donnelly *et al.*, 1990). Two magmatic suites are unrelated to subduction: (1) Jurassic to Upper Cretaceous, mainly Turonian, MORB and OIB lavas (Sinton *et al.*, 1998; Révillon *et al.*, 2000; Kerr *et al.*, 2003) thought to be portions of the Caribbean–Colombian oceanic plateau (Kerr *et al.*, 1997; Lapierre *et al.*, 1999, 2000; Mamberti *et al.*, 2003, and references therein), or pieces of the Proto-Caribbean (Atlantic) oceanic crust (Kerr *et al.*, 1997); (2) middle Tertiary to Holocene alkaline basalt suites associated with extensional tectonics. The third type of igneous activity comprises subduction-related volcanic and plutonic rocks spanning the interval from the Early Cretaceous to the Holocene, which are associated with the development of the Greater and Lesser Antilles arcs. These suites include Lower Cretaceous island arc tholeiite (IAT) and many Cenomanian–Holocene calcalkaline and minor high-K series. The change from IAT to calcalkaline magmatism is attributed either to a gradual transition related to the maturation of the arc(s) (Kerr *et al.*, 2003) or to an abrupt switch of magmatism as a result of a polarity reversal of subduction (Lebron & Perfit, 1993, 1994; Draper *et al.*, 1996). In the Greater Antilles Island Arc the calcalkaline igneous activity continued until the Eocene, and in the Lesser Antilles it persists to the present.

The Cuban Cretaceous arc rocks (Fig. 1a) constitute the westernmost part of the extinct Greater Antilles

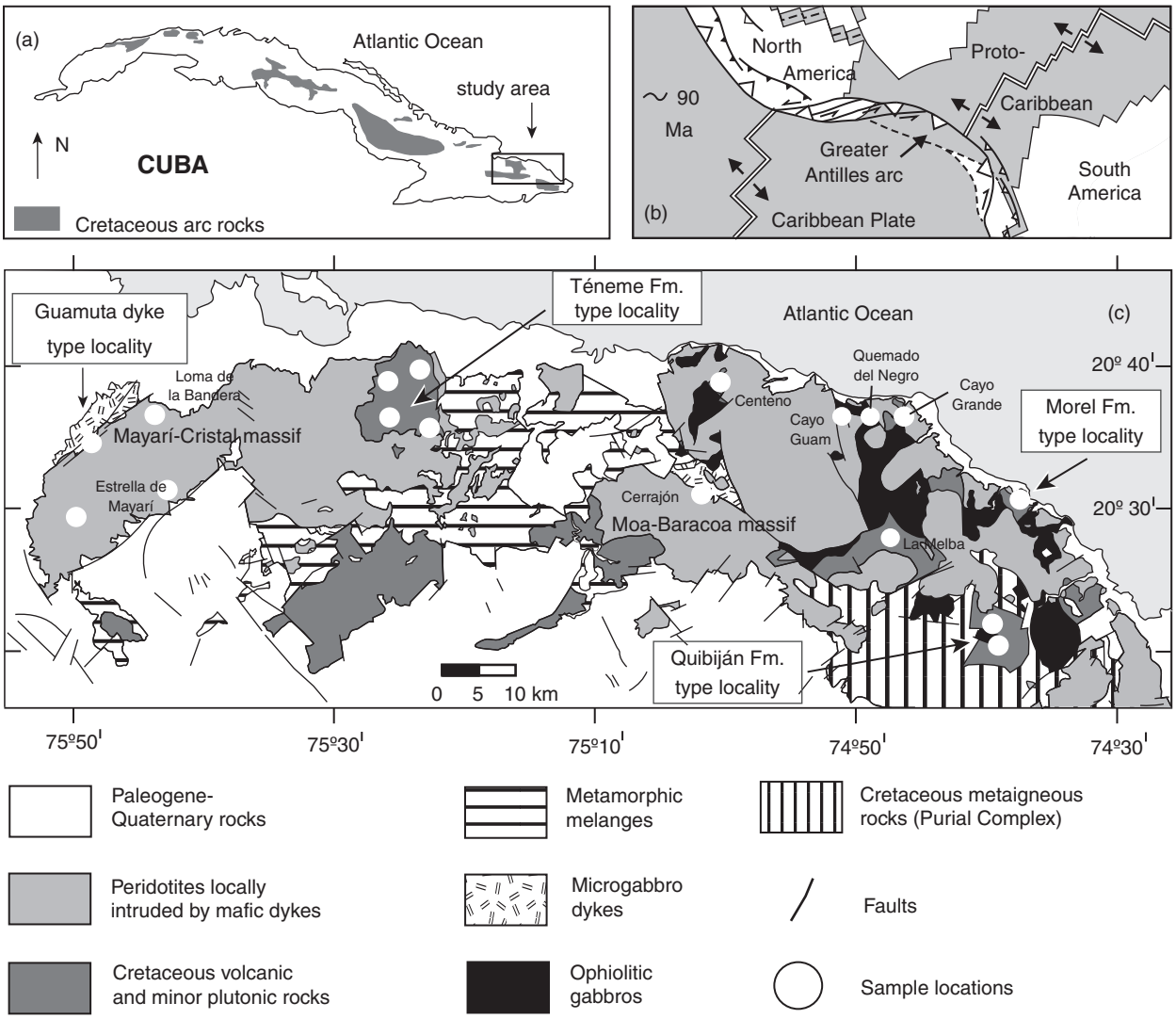

Fig. 1. (a) Geographical location of Cretaceous arc rocks in Cuba (Iturralde-Vinent, 1998); rectangle indicates the study area. (b) Middle–Late Cretaceous paleotectonic reconstruction of the Caribbean realm, modified from Pindell & Kennan (2001). (c) Geological map of eastern Cuba showing the location of the studied samples.

Island Arc (Fig. 1b). In eastern Cuba the Cretaceous volcanic rocks form the Quibiján, Téneme and the Santo Domingo Formations (Iturralde-Vinent, 1996*a*, 1996*b*, and references therein; Gyarmati *et al.*, 1998; Kerr *et al.*, 1999). The first two formations were sampled for this study (Fig. 1c). The Quibiján lavas mainly consist of massive, porphyritic and quartz–chlorite-filled amygdaloidal basalt, basaltic andesite and minor andesite, interbedded with chert and fine-grained tuffaceous rocks. Iturralde-Vinent *et al.* (2006) proposed an Albian–Turonian age for the Quibiján Formation. The Turonian–Coniacian pillow basalt and basaltic andesite from the locality of Morel (Fig. 1c) (Iturralde-Vinent *et al.*, 2006) have been previously included in the Quibiján volcanic rocks and classified as back-arc IAT (Kerr *et al.*, 1999). As we will argue below, however, several units initially assigned to the Quibiján Formation have distinctive geochemical signatures such that their inclusion within a single volcanic formation is inappropriate (see also Proenza *et al.*, 2006). The Téneme Formation mainly consists of basalt, basaltic andesite, andesite and minor dacite (Proenza *et al.*, 2006) interbedded with tuff, tuffaceous sandstone, and limestone of Turonian–Early Coniacian age (Iturralde-Vinent *et al.*, 2006). The Téneme extrusives are classified as IAT related to early island arc magmatism (Proenza *et al.*, 2006).

PETROGRAPHY AND SAMPLING

For this study we selected 57 igneous rocks from several localities in eastern Cuba (Fig. 1c). We chose only the least

altered specimens on the basis of their petrography and whole-rock compositions. Moreover, we excluded samples with petrographic and major-element evidence of phenocryst accumulation.

Major mineral phases include plagioclase, clinopyroxene, iron–titanium oxides, ± minor hornblende, quartz, orthopyroxene and rare olivine. Volcanic rocks have micro-crystalline or porphyritic–aphanitic textures with clinopyroxene and plagioclase phenocrysts. Subvolcanic dykes generally have fine phaneritic (<1 mm) homogeneous texture. Accessory minerals include epidote, apatite and sulphides. Primary phases underwent hydrothermal alteration under greenschist-facies conditions. Albitized plagioclase grains are commonly altered to sericite, saussurite, chlorite or smectite, and clinopyroxene is replaced by hornblende and chlorite. Secondary veins consist of quartz–celadonite, sericite, serpentine, carbonate and Fe-oxyhydroxides. Intrusive rock from the Téneme Formation consists of 200–800 μm plagioclase, quartz and Fe–Ti oxides, and 2–3 mm amphibole and quartz megacrysts.

We selected 28 samples from the western part of the studied area (Fig. 1c), where igneous suites are in tectonic contact with the Mayarí–Cristal ophiolitic massif, of which 14 volcanic rocks are from the type locality of the Téneme Formation. Eleven of the Téneme samples were previously studied by Proenza *et al.* (2006) and have been reanalysed here for trace-element abundances and radiogenic isotope ratios. In addition, we analysed one sample of the Téneme intrusive, 11 subvolcanic dykes collected in the NW region of the Mayarí–Cristal massif (Guamuta–Loma de la Bandera area), and two dykes from the Estrella de Mayarí area, all of which are intrusive into mantle peridotite. From the eastern domain, where igneous suites are spatially associated with the Moa–Baracoa ophiolitic rocks, we selected 29 samples (Fig. 1c), of which 16 volcanic rocks are from the area of the Barbudo and Quibiján Rivers where the homonymous formation was originally defined (Quintas, 1988). In addition, we analysed six pillow lavas from the localities of Morel and Centeno, two volcanic rocks from La Melba area, and one mafic dyke that intrudes into mantle peridotite in the Cerrajón region. Finally, we selected one pillow lava from Morel previously studied by Proenza *et al.* (2006), and three olivine gabbros from the crustal section (in Cayo Grande and Quemado del Negro) and Moho transition zone (in Cayo Guam) of the Moa–Baracoa ophiolitic massif, studied by Marchesi *et al.* (2006) and analysed here for radiogenic isotope ratios.

ANALYTICAL METHODS

Whole-rock major- and trace-element analyses

Samples were sawn into thin slabs and secondary veins were carefully removed. Whole-rock powders were obtained from sample aliquots by first crushing and then powdering large amounts of the sample (usually >3 kg) in an agate ring mill. Whole-rock major- and minor-transition elements (Sc, V, Cr and Ni) were analysed in a single low (2:1) Li-tetraborate ($Li_2B_4O_7$) fused bead by a ThermoARL Advant XP+ sequential X-ray fluorescence (XRF) spectrometer at the GeoAnalytical Lab facilities of the Washington State University (WSU; Pullman, WA, USA). Details of the analytical procedure have been given by Johnson *et al.* (1999).

Whole-rock trace elements (Rb, Sr, Y, Zr, Nb, Cs, Ba, REE, Hf, Ta, Pb, Th and U) were analysed by inductively coupled plasma mass spectrometry (ICP-MS) at the GeoAnalytical Lab of the WSU using an HP 4500+ system. Rock powder (2 g) was mixed with an equal amount of lithium tetraborate flux, placed into a carbon crucible and fused in a 1000°C muffle furnace for 30 min. The resulting fusion bead was briefly ground in a shatterbox swing agate mill and 250 mg of this powder was dissolved on a hotplate at 110°C in a mixture of HF, HNO_3, and $HClO_4$ in an open Teflon vial and then evaporated. One acid blank and two samples each of three in-house rock standards were run with each analytical batch. Whole-rock geochemical data are given in Table 1. Results for the BHVO-1 and AN-G international reference materials run as unknowns for 1 year at the WSU GeoAnalytical Laboratory are also shown. The concentrations of the analyzed standards show good agreement with working values for the reference samples; for example, Nb/Ta differs by only ~10% from the recommended values (Govindaraju, 1994). The reproducibility at the WSU GeoAnalytical Laboratory is indicated by the analyses of the TED in-house standard (primitive basalt from the Oregon Cascade range) repeated over a period of 3 years. Precision is better than 10% for all the analyzed elements. To assess the quality of the Nb and Ta data, replicate analyses of four Quibiján samples were performed at the Géosciences Montpellier laboratory (CNRS-Université Montpellier II, Montpellier, France) with a ThermoFinnigan ELEMENT XR high resolution (HR)-ICP-MS system using the dissolution procedure described by Garrido *et al.* (2000). Nb/Ta ratios of replicate analyses are within analytical errors and differ by less than 11% from the values obtained at WSU (Table 1).

Analyses of radiogenic isotope ratios

Nd, Sr and Pb radiogenic isotope ratios were measured in whole-rocks and, for some samples, in clinopyroxene and plagioclase mineral separates. Specimens selected for isotope analyses include 15 volcanic rocks (10 from the Téneme and Quibiján Formations, three from the Centeno and two from the Morel areas), six subvolcanic dykes from the Guamuta–Loma de la Bandera and one from the Estrella de Mayarí areas, one sample of the

Table 1: Whole-rock major- and trace-element data for igneous rocks from eastern Cuba

Group:	Group 1									Group 2											
Type:	Morel volcanics				La Melba volcanics		Centeno volcanics			Guamuta dykes						Loma de la Bandera dykes					Cerrajón dyke
Lat. N:	20°29′19″				20°28′03″		20°38′33″		20°37′53″	20°34′49″	20°34′41″	20°34′44″	20°34′21″	20°33′57″	20°32′56″	20°35′31″	20°35′23″	20°35′08″	20°35′54″	20°35′47″	20°31′10″
Long. W:	74°38′06″				74°47′43″		74°59′42″		75°00′34″	75°48′29″	75°48′20″	75°48′19″	75°48′28″	75°48′04″	75°47′46″	75°43′14″	75°43′16″	75°43′16″	75°43′10″	75°43′08″	75°01′23″
Sample:	M 200	M 201	M 202	MOREL 1[1]	MEL 200	MEL 201	CEN 200	CEN 201	CEN 202	GUA 200	GUA 201	GUA 202	GUA 203	GUA 205	GUA 206	LB 200	LB 201	LB 202	LB 203	LB 204	FA 202
wt%																					
SiO_2	49·59	51·12	49·08	47·35	49·83	49·11	52·66	51·05	49·23	51·75	49·19	51·64	50·69	50·83	52·12	50·64	50·50	56·33	50·35	43·05	51·65
TiO_2	1·95	1·87	1·88	1·77	1·21	2·17	2·33	2·17	2·87	1·04	0·94	0·89	0·82	0·82	1·41	0·78	0·89	0·70	0·84	1·41	0·80
Al_2O_3	14·35	14·16	14·38	14·01	14·87	13·64	12·79	13·54	13·11	16·28	16·63	15·84	16·81	16·22	16·49	16·37	16·40	16·23	15·75	16·64	15·93
FeO*	10·91	10·67	11·04	10·12	9·67	13·19	12·78	11·60	14·31	8·56	9·44	8·88	8·20	7·71	10·33	8·08	8·62	9·50	8·38	6·21	7·71
MnO	0·20	0·18	0·22	0·19	0·14	0·26	0·21	0·21	0·28	0·15	0·18	0·18	0·14	0·14	0·18	0·16	0·16	0·16	0·15	0·14	0·16
MgO	7·91	7·98	8·16	7·20	8·37	7·20	4·79	6·58	6·90	7·74	7·86	8·08	8·45	8·36	5·87	8·30	8·39	5·47	9·09	12·83	8·92
CaO	9·54	8·33	9·77	12·25	10·83	9·09	7·88	8·20	8·12	11·51	10·63	9·82	12·80	13·04	9·65	12·54	11·47	8·49	12·33	15·59	11·13
Na_2O	3·07	3·06	2·82	1·71	3·22	3·79	3·71	4·51	2·93	2·90	3·65	3·29	1·78	2·18	2·96	2·30	2·65	2·89	2·37	0·67	2·91
K_2O	0·79	0·94	1·24	0·50	0·40	0·16	0·36	0·21	0·59	0·08	0·04	0·36	0·02	0·06	0·54	0·12	0·14	0·17	0·12	0·05	0·07
P_2O_5	0·19	0·17	0·18	0·16	0·10	0·20	0·44	0·21	0·29	0·08	0·08	0·07	0·06	0·06	0·10	0·06	0·07	0·06	0·06	0·67	0·07
Total	98·50	98·48	98·77	95·26	98·64	98·81	97·96	98·26	98·64	100·09	98·63	99·04	99·78	99·42	99·66	99·36	99·29	100·00	99·45	97·26	99·37
ppm																					
Sc	45	46	45	n.a.	40	44	36	42	44	38	40	41	38	41	37	39	40	34	41	35	32
V	380	364	375	359	271	394	279	399	486	248	277	257	229	240	369	237	253	305	236	227	215
Cr	144	166	167	161	386	125	67	125	85	253	184	153	318	170	13	167	210	26	406	99	324
Ni	56	57	59	58	89	52	32	57	42	76	70	62	102	82	35	75	73	22	111	289	141
Rb	8·5	9·9	11	5·1	1·8	0·77	1·9	2·1	2·7	0·30	0·20	1·8	0·12	0·47	3·6	0·87	1·2	0·98	1·2	0·36	0·77
Sr	97	111	107	58	181	133	93	67	122	128	80	164	109	117	173	145	198	164	151	59	179
Y	45	40	42	37	28	48	100	49	64	25	23	20	20	20	29	19	22	17	20	53	21
Zr	116	108	110	108	64	130	348	134	187	62	46	40	43	42	64	37	44	35	41	54	46
Nb	3·2	2·9	2·9	3·0	1·4	3·6	8·3	3·6	5·7	0·57	0·64	0·63	0·48	0·48	0·98	0·47	0·53	0·38	0·56	1·3	0·40
Cs	0·18	0·19	0·36	0·15	0·058	0·013	0·021	0·012	0·031	b.d.l.	b.d.l.	0·0003	b.d.l.	0·008	0·018	0·008	0·028	0·029	0·086	0·018	0·031

(continued)

Table 1: Continued

Group:	Group 1									Group 2										
Type:	Morel volcanics				La Melba volcanics		Centeno volcanics			Guamuta dykes						Loma de la Bandera dykes					Cerrajón dyke
Sample:	M 200	M 201	M 202	MOREL 1[1]	MEL 200	MEL 201	CEN 200	CEN 201	CEN 202	GUA 200	GUA 201	GUA 202	GUA 203	GUA 205	GUA 206	LB 200	LB 201	LB 202	LB 203	LB 204	FA 202
Ba	11	12	14	8·0	14	6·5	8·5	15	19	16	5·7	43	8·7	17	54	26	42	62	25	5·5	8·1
La	4·1	3·9	3·8	3·7	2·4	4·9	12	5·0	7·4	2·2	2·0	1·7	1·6	1·6	2·7	1·4	1·8	1·8	1·5	5·6	1·6
Ce	12	12	11	12	7·2	14	35	15	21	6·8	5·6	4·9	4·8	4·8	7·7	4·3	5·2	4·5	4·5	17	5·0
Pr	2·1	1·9	1·9	2·1	1·2	2·3	5·6	2·4	3·3	1·2	0·94	0·83	0·83	0·83	1·3	0·73	0·89	0·72	0·77	3·0	0·88
Nd	12	11	11	11	6·9	13	31	14	18	6·5	5·4	4·8	4·8	4·7	7·3	4·4	5·2	4·1	4·6	18	5·3
Sm	4·7	4·2	4·3	4·1	2·7	5·0	11	5·2	6·8	2·6	2·2	2·0	2·0	1·9	3·0	1·9	2·1	1·7	2·0	6·5	2·1
Eu	1·7	1·5	1·5	1·4	1·1	1·7	3·3	1·8	2·3	1·0	0·88	0·81	0·82	0·79	1·2	0·77	0·80	0·69	0·81	1·7	0·87
Gd	6·3	5·6	5·8	5·3	3·8	6·7	14	7·0	8·9	3·5	3·1	2·8	2·8	2·7	4·1	2·6	3·0	2·3	2·7	8·1	2·9
Tb	1·2	1·1	1·1	0·91	0·72	1·3	2·7	1·3	1·7	0·66	0·59	0·54	0·53	0·52	0·77	0·51	0·56	0·44	0·53	1·5	0·56
Dy	7·9	7·3	7·5	6·2	4·9	8·5	18	8·7	11	4·4	4·1	3·6	3·6	3·4	5·1	3·4	3·8	2·9	3·6	9·6	3·8
Ho	1·7	1·5	1·6	1·4	1·0	1·8	3·8	1·9	2·4	0·93	0·88	0·78	0·77	0·75	1·1	0·74	0·81	0·65	0·77	2·0	0·80
Er	4·6	4·2	4·4	3·8	2·9	5·0	11	5·2	6·7	2·6	2·4	2·2	2·1	2·1	3·1	2·0	2·3	1·9	2·1	5·5	2·2
Tm	0·65	0·59	0·63	0·57	0·42	0·73	1·5	0·73	0·96	0·37	0·35	0·31	0·31	0·30	0·44	0·30	0·32	0·27	0·30	0·77	0·32
Yb	4·1	3·8	3·9	3·6	2·6	4·5	9·6	4·6	5·9	2·3	2·2	1·9	1·9	1·9	2·8	1·8	2·0	1·7	1·9	4·6	2·0
Lu	0·64	0·60	0·62	0·49	0·41	0·70	1·5	0·71	0·93	0·37	0·35	0·30	0·31	0·30	0·44	0·29	0·32	0·29	0·30	0·69	0·31
Hf	3·3	3·1	3·1	3·0	1·9	3·7	9·4	3·8	5·2	1·9	1·4	1·3	1·3	1·3	2·0	1·2	1·4	1·2	1·3	2·1	1·4
Ta	0·24	0·21	0·23	n.a.	0·11	0·27	0·61	0·27	0·43	0·051	0·048	0·051	0·042	0·037	0·077	0·035	0·041	0·029	0·043	0·085	0·033
Pb	0·55	0·48	0·59	0·38	0·074	0·20	0·53	0·49	0·98	0·26	0·22	0·15	0·24	0·20	0·45	0·56	0·17	0·21	0·21	0·15	0·22
Th	0·19	0·18	0·18	0·17	0·091	0·23	0·63	0·24	0·38	0·10	0·15	0·13	0·076	0·092	0·17	0·064	0·12	0·26	0·077	0·084	0·11
U	0·32	0·30	0·44	0·27	0·032	0·078	0·24	0·15	0·14	0·041	0·051	0·046	0·025	0·035	0·068	0·030	0·046	0·11	0·027	0·16	0·034

(continued)

Table 1: Continued

Group:	Group 3																
Subgroup:	3T																
Type:	Téneme volcanics										Téneme volcanics with boninitic affinity				Téneme intrusive	Estrella de Mayarí dykes	
Lat. N:	20°38′50″	20°39′07″	20°38′50″						20°40′10″		20°39′35″		20°39′10″		20°35′58″	20°27′46″	20°30′49″
Long. W:	75°25′43″	75°25′32″	75°25′43″						75°23′05″		75°25′55″		75°25′45″		75°22′31″	75°50′16″	75°42′04″
Sample:	T 200	T 201	T 202	TEN 1[1]	TEN 2[2]	TEN 3[1]	TM 12[2]	TM 13[2]	TM 20[2]	TM 21[1]	TM 1[1]	TM 8[2]	TM 14[2]	TM 15[2]	DT 200	CAR 4	LEM 5
wt%																	
SiO_2	55·64	55·20	58·59	55·45	57·63	67·27	68·61	66·78	58·19	50·51	55·95	59·75	54·53	56·09	61·01	51·76	51·15
TiO_2	0·43	0·92	0·42	0·46	0·40	0·73	0·76	0·76	0·45	0·83	0·28	0·39	0·37	0·35	0·49	0·62	0·63
Al_2O_3	18·33	16·47	16·69	18·86	15·73	13·51	13·60	13·34	14·55	17·68	12·77	15·39	14·23	13·18	17·38	19·81	18·87
FeO*	8·05	9·88	7·07	6·33	6·16	6·14	4·99	6·16	6·71	9·39	6·69	5·94	7·20	6·98	6·92	7·91	8·56
MnO	0·04	0·18	0·09	0·11	0·11	0·07	0·08	0·08	0·12	0·19	0·13	0·08	0·13	0·13	0·17	0·15	0·15
MgO	5·41	3·88	5·28	4·27	5·15	0·89	0·87	1·12	5·59	4·88	9·17	7·73	8·00	8·24	2·88	3·38	3·73
CaO	6·69	8·11	8·69	7·84	9·05	2·34	2·80	2·86	10·06	8·04	8·32	0·49	9·24	8·85	7·25	7·18	10·44
Na_2O	1·70	3·56	2·03	2·79	1·69	5·96	6·00	5·37	1·51	3·29	2·69	4·49	1·42	1·42	2·52	4·36	2·47
K_2O	1·05	0·81	0·53	0·50	0·25	1·44	0·66	1·02	0·22	0·85	0·28	0·22	0·71	0·65	0·51	1·00	0·64
P_2O_5	0·05	0·13	0·06	0·08	0·06	0·20	0·21	0·19	0·06	0·10	0·03	0·07	0·05	0·07	0·11	0·15	0·13
Total	97·38	99·14	99·44	96·69	96·23	98·55	98·58	97·68	97·46	95·76	96·31	94·55	95·88	95·96	99·24	96·32	96·78
ppm																	
Sc	28	34	34	n.a.	n.a.	n.a.	n.a.	n.a.	n.a.	n.a.	n.a.	n.a.	n.a.	n.a.	27	n.a.	n.a.
V	189	316	204	190	170	70	81	80	199	325	185	218	187	175	139	268	318
Cr	65	15	109	45	171	27	59	90	194	51	500	94	293	296	3·9	25	31
Ni	56	11	34	27	49	11	21	34	58	22	113	22	59	62	6·2	20	14
Rb	7·1	9·7	6·5	5·4	4·3	n.a.	7·8	13	3·0	8·4	3·2	2·2	8·3	8·4	10	11	5·4
Sr	307	259	238	582	334	n.a.	97	110	279	324	292	63	348	248	112	496	494
Y	12	23	15	16	13	n.a.	38	33	14	20	13	17	8·9	10	16	12	9·7
Zr	51	61	37	59	47	n.a.	116	116	50	40	28	48	42	52	45	28	29
Nb	0·69	0·62	1·5	1·2	1·0	n.a.	1·8	1·7	0·60	1·3	1·2	0·61	0·64	0·71	1·5	1·1	1·0
Cs	0·36	0·15	0·20	0·30	0·13	n.a.	0·036	0·080	0·065	0·22	0·17	0·19	0·094	0·14	0·60	0·10	0·089
Ba	5157	307	284	627	223	n.a.	247	312	67	421	116	78	137	311	258	339	217
La	3·8	5·0	3·7	7·6	6·3	n.a.	12	12	4·8	4·1	1·6	10	3·5	6·3	6·0	4·4	4·2
Ce	8·2	12	7·6	17	13	n.a.	27	26	11	12	4·8	20	7·6	14	12	10	10
Pr	1·1	1·8	1·0	2·3	1·6	n.a.	3·8	3·7	1·6	1·7	0·65	2·6	1·0	1·9	1·5	1·5	1·4
Nd	5·2	9·5	4·6	9·7	7·2	n.a.	19	18	7·6	8·5	2·8	11	4·9	8·7	6·7	7·9	6·9

(continued)

Table 1: Continued

Group:	Group 3															
Subgroup:	3T															
Type:	Téneme volcanics										Téneme volcanics with boninitic affinity				Téneme intrusive	Estrella de Mayarí dykes	
Sample:	T 200	T 201	T 202	TEN 1[1]	TEN 2[2]	TEN 3[1]	TM 12[2]	TM 13[2]	TM 20[2]	TM 21[1]	TM 1[1]	TM 8[2]	TM 14[2]	TM 15[2]	DT 200	CAR 4	LEM 5
Sm	1·7	3·2	1·5	2·3	1·9	n.a.	5·4	5·2	2·3	2·5	0·95	2·8	1·5	2·2	2·0	2·1	1·8
Eu	0·54	1·1	0·54	0·98	0·64	n.a.	1·5	1·4	0·79	0·91	0·39	1·1	0·50	0·76	0·73	0·79	0·69
Gd	1·8	3·6	1·9	2·4	2·1	n.a.	5·9	5·6	2·4	2·9	1·3	3·0	1·5	2·1	2·2	2·4	2·0
Tb	0·31	0·61	0·36	0·38	0·35	n.a.	0·99	0·94	0·40	0·50	0·23	0·46	0·26	0·32	0·40	0·37	0·33
Dy	2·0	4·0	2·4	2·4	2·3	n.a.	6·3	5·9	2·5	3·0	1·5	2·8	1·6	1·9	2·7	2·6	2·2
Ho	0·45	0·85	0·55	0·53	0·49	n.a.	1·3	1·2	0·52	0·64	0·33	0·58	0·34	0·39	0·58	0·55	0·48
Er	1·3	2·4	1·6	1·5	1·4	n.a.	3·7	3·4	1·4	1·8	0·95	1·6	0·95	1·1	1·7	1·5	1·3
Tm	0·20	0·35	0·24	0·24	0·21	n.a.	0·56	0·50	0·21	0·27	0·15	0·24	0·14	0·16	0·26	0·23	0·20
Yb	1·3	2·2	1·6	1·5	1·4	n.a.	3·4	3·2	1·4	1·7	1·0	1·5	0·90	1·0	1·8	1·5	1·3
Lu	0·22	0·34	0·26	0·25	0·23	n.a.	0·55	0·51	0·22	0·26	0·16	0·25	0·15	0·16	0·30	0·25	0·22
Hf	1·7	2·0	1·3	1·8	1·5	n.a.	3·8	3·8	1·6	3·3	3·1	1·5	1·3	1·6	1·6	1·1	1·1
Ta	0·044	0·047	0·11	n.a.	0·051	n.a.	0·10	0·093	0·042	n.a.	n.a.	0·041	0·039	0·044	0·11	0·092	0·084
Pb	3·2	1·1	2·4	3·6	3·0	n.a.	3·6	1·5	3·1	2·4	1·9	2·4	2·0	2·7	1·1	1·4	2·1
Th	0·77	0·57	0·53	0·87	0·76	n.a.	1·5	1·5	0·57	0·58	0·46	0·70	0·55	1·1	1·2	0·42	0·45
U	0·96	0·42	0·45	0·65	0·57	n.a.	1·1	1·0	0·41	0·38	0·38	0·44	0·24	0·50	0·50	0·24	0·29

Table 1: Continued

Group:	Group 3															
Subgroup:	3Q															
Type:	Quibiján volcanics (Q1)												Quibiján volcanics (Q2)			
Lat. N:	20°20′41″		20°20′35″		20°20′40″		20°20′41″		20°21′05″	20°20′49″			20°20′41″	20°20′41″		20°20′59″
Long. W:	74°39′29″		74°39′59″		74°39′58″		74°39′46″		74°39′19″	74°39′35″			74°39′29″	74°39′39″		74°39′23″
Sample:	Q 200	Q 201	Q 203	Q 204	Q 205	Q 206	Q 207	Q 208	Q 212	Q 213	Q 214	Q 215	Q 202	Q 209	Q 210	Q 211
wt%																
SiO_2	46·40	51·84	47·56	58·28	46·93	51·59	44·67	46·88	51·70	47·30	50·84	48·51	50·53	50·60	55·05	52·62
TiO_2	0·65	0·55	0·69	0·69	0·73	0·67	0·54	0·56	0·85	0·60	0·73	0·69	0·57	0·57	0·85	0·66
Al_2O_3	18·54	18·01	18·74	17·12	18·47	17·70	17·72	18·07	17·12	17·28	20·00	19·24	14·60	17·29	18·08	16·54
FeO*	8·29	7·30	8·89	7·26	7·93	10·48	9·21	7·54	9·53	8·18	8·35	8·42	8·63	8·53	8·26	9·14
MnO	0·16	0·13	0·15	0·12	0·17	0·12	0·16	0·17	0·12	0·17	0·10	0·14	0·17	0·16	0·12	0·18
MgO	5·92	6·02	5·88	3·84	5·07	6·94	5·23	4·43	5·03	6·11	4·97	5·13	9·71	7·06	3·99	6·18
CaO	13·18	9·74	11·38	6·83	13·67	7·26	15·12	17·92	8·80	12·64	9·52	11·69	11·46	11·59	6·70	9·85
Na_2O	2·31	4·82	1·99	3·02	2·00	1·23	2·24	2·77	4·50	2·31	2·28	2·04	1·80	1·80	5·49	3·21
K_2O	0·88	0·17	1·03	1·29	0·86	1·35	0·31	0·27	0·65	0·72	0·69	0·81	0·83	1·36	0·35	0·84
P_2O_5	0·07	0·09	0·07	0·20	0·08	0·06	0·07	0·07	0·11	0·08	0·08	0·08	0·06	0·06	0·14	0·08
Total	96·40	98·68	96·38	98·64	95·91	97·39	95·28	98·67	98·40	95·39	97·57	96·73	98·35	99·01	99·03	99·30
ppm																
Sc	36	37	34	31	35	43	39	38	37	36	32	36	45	39	27	38
V	253	255	251	210	251	318	266	268	289	232	246	248	250	246	286	277
Cr	64	56	45	17	28	37	117	85	62	101	25	54	353	174	13	62
Ni	28	42	38	14	15	38	46	30	27	34	22	41	91	45	16	34
Rb	11	1·7	12	17	11	15	6·4	4·1	8·2	8·3	8·7	11	10	19	6·6	15
Sr	218	327	168	218	162	294	167	134	309	215	239	220	297	325	394	277
Y	15	14	17	23	18	13	13	13	21	15	17	17	16	17	22	20
Zr	35	33	46	53	44	34	33	31	62	36	46	43	35	37	71	47
Nb	0·44	0·38	0·59	0·70	0·68	0·36	0·40	0·36	0·78	0·43	0·67	0·58	1·0	1·0	1·6	1·6
Nb[3]						0·36		0·37						1·0		1·6
Cs	0·34	0·032	0·30	0·33	0·37	0·63	0·14	0·092	0·15	0·29	0·28	0·33	0·12	0·33	0·070	0·20
Ba	177	131	203	277	171	709	66	54	152	181	196	208	311	562	109	230
La	3·2	3·0	3·9	5·5	3·9	2·9	3·3	3·1	5·9	3·2	3·6	3·7	4·0	4·6	8·5	4·7
Ce	7·5	7·0	9·3	13	9·1	6·9	7·3	7·3	14	7·5	8·6	8·6	8·4	9·3	18	9·6
Pr	1·1	1·0	1·4	1·8	1·4	1·0	1·1	1·1	1·9	1·1	1·3	1·3	1·2	1·2	2·4	1·3

(continued)

Table 1: Continued

Group:	Group 3														
Subgroup:	3Q														
Type:	Quibiján volcanics (Q1)												Quibiján volcanics (Q2)			
Sample:	Q 200	Q 201	Q 203	Q 204	Q 205	Q 206	Q 207	Q 208	Q 212	Q 213	Q 214	Q 215	Q 202	Q 209	Q 210	Q 211
Nd	5·9	5·5	6·9	9·2	6·9	5·4	5·4	5·5	9·4	5·8	6·6	6·6	5·8	5·9	11	6·4
Sm	2·0	1·8	2·2	2·9	2·2	1·8	1·8	1·7	2·9	1·9	2·2	2·1	1·9	2·0	3·3	2·3
Eu	0·75	0·68	0·80	0·88	0·85	0·69	0·68	0·64	0·96	0·64	0·78	0·79	0·71	0·70	1·1	0·81
Gd	2·4	2·2	2·5	3·4	2·7	2·1	2·0	2·0	3·3	2·2	2·5	2·5	2·4	2·3	3·6	2·8
Tb	0·42	0·37	0·45	0·59	0·48	0·37	0·34	0·34	0·58	0·40	0·46	0·45	0·44	0·44	0·60	0·51
Dy	2·7	2·4	3·0	3·8	3·1	2·4	2·2	2·2	3·8	2·6	3·1	2·9	2·9	2·9	3·9	3·4
Ho	0·57	0·51	0·65	0·82	0·67	0·52	0·47	0·48	0·80	0·56	0·66	0·62	0·61	0·63	0·83	0·74
Er	1·6	1·4	1·8	2·3	1·8	1·4	1·4	1·3	2·2	1·6	1·8	1·7	1·7	1·8	2·3	2·1
Tm	0·23	0·21	0·26	0·32	0·27	0·21	0·19	0·19	0·33	0·23	0·26	0·25	0·26	0·26	0·34	0·31
Yb	1·5	1·3	1·6	2·0	1·7	1·3	1·2	1·2	2·0	1·4	1·6	1·6	1·7	1·6	2·1	2·0
Lu	0·23	0·21	0·27	0·32	0·28	0·21	0·19	0·19	0·32	0·22	0·27	0·25	0·26	0·27	0·34	0·31
Hf	1·2	1·1	1·4	1·7	1·4	1·1	1·0	0·99	1·9	1·1	1·4	1·3	1·2	1·2	2·2	1·6
Ta	0·032	0·022	0·037	0·047	0·044	0·027	0·025	0·025	0·055	0·032	0·049	0·041	0·11	0·12	0·15	0·21
Ta[3]						0·030		0·028						0·12		0·19
Pb	1·8	1·2	1·9	1·7	1·5	1·3	1·3	1·5	4·1	1·2	1·4	1·8	4·7	18	6·5	3·5
Th	0·33	0·34	0·52	0·58	0·41	0·32	0·43	0·39	0·70	0·36	0·46	0·44	0·94	1·1	1·6	1·5
U	0·21	0·20	0·33	0·57	0·27	0·19	0·73	0·34	0·60	0·23	0·26	0·28	0·65	0·66	0·91	0·84

(continued)

Table 1: Continued

Group:	Moa-Baracoa ophiolitic gabbros			ICP-MS standards					
Subgroup:	Crustal gabbros		MTZ sill	BHVO-1		AN-G		TED	
Type:	Cayo Grande	Quemado del Negro	Cayo Guam	WSU	Govin. 1994	WSU	Govin. 1994	WSU ($n=54$)	RSD (%)
Sample	CY 200	QN 4[4]	CG 17[4]						
Lat. N:	20°35′15″	20°35′30″	20°35′45″						
Long. W:	74°46′34″	74°49′10″	74°51′23″						
wt%									
SiO_2	50·65	50·00	41·06						
TiO_2	0·66	0·29	0·21						
Al_2O_3	16·40	16·85	6·30						
FeO*	8·14	5·49	11·46						
MnO	0·16	0·11	0·19						
MgO	7·59	11·05	27·59						
CaO	12·88	15·71	5·19						
Na_2O	2·75	1·37	0·45						
K_2O	0·11	b.d.l.	b.d.l.						
P_2O_5	0·03	0·01	0·01						
Total	99·37	100·88	92·45						
ppm									
Sc	44	n.a.	n.a.						
V	235	157	108						
Cr	515	855	2275						
Ni	95	243	1400						
Rb	0·57	0·046	0·089	10	11	1·7	1	4·1	8
Sr	147	78	38	394	403	78	76	208	2
Y	19	7·3	4·4	28	28	8·5	7·5	29	2
Zr	22	5·3	3·5	n.av.	179	n.av.	11	61	2
Nb	0·32	0·053	0·012	18	19	0·86	0·7	2·6	4
Nb[3]									
Cs	b.d.l.	0·003	0·007	0·12	0·13	0·18	0·05	0·10	9
Ba	7·6	3·3	2·1	133	139	32	34	71	2
La	0·88	0·26	0·16	15·7	15·8	2·4	2·2	4·2	3
Ce	2·9	0·92	0·56	37	39	4·6	4·7	9·8	2
Pr	0·52	0·19	0·11	5·5	5·7	0·7	0·6	1·6	2
Nd	3·3	1·3	0·75	25	25·2	2·5	2·4	8·2	2
Sm	1·6	0·59	0·34	6·2	6·2	0·73	0·70	3·0	2
Eu	0·90	0·38	0·21	2·1	2·06	0·36	0·37	1·2	2
Gd	2·4	1·0	0·59	6·3	6·40	1·0	0·90	4·0	2
Tb	0·48	0·19	0·11	0·96	0·96	0·19	0·20	0·75	2
Dy	3·3	1·4	0·85	5·2	5·20	1·2	1·20	5·0	1
Ho	0·72	0·30	0·19	0·93	0·99	0·26	0·27	1·1	2
Er	2·0	0·83	0·56	2·4	2·40	0·76	0·75	3·1	2
Tm	0·29	0·12	0·083	0·34	0·33	0·12	0·12	0·46	2
Yb	1·8	0·75	0·56	2·0	2·02	0·80	0·75	2·9	1
Lu	0·28	0·12	0·094	0·28	0·29	0·13	0·12	0·46	2

(continued)

Table 1: Continued

Group:	Moa-Baracoa ophiolitic gabbros			ICP-MS standards					
Subgroup:	Crustal gabbros		MTZ sill	BHVO-1		AN-G		TED	
Type:	Cayo Grande	Quemado del Negro	Cayo Guam	WSU	Govin. 1994	WSU	Govin. 1994	WSU ($n=54$)	RSD (%)
Sample	CY 200	QN 4[4]	CG 17[4]						
Hf	0·79	0·24	0·16	4·3	4·38	0·40	0·38	1·9	2
Ta	0·024	0·013	0·001	1·2	1·23	0·25	0·18	0·17	6
Ta[3]									
Pb	0·46	0·14	0·11	n.av.	2·6	n.av.	2	0·87	8
Th	0·019	0·003	0·001	1·3	1·08	0·071	0·04	0·40	8
U	0·008	0·001	b.d.l.	0·39	0·42	0·039	0·12	0·14	7

ICP-MS results for international reference materials (BHVO-1; AN-G) and TED in-house standard run as unknowns at the Washington State University (WSU) GeoAnalytical Laboratory are also shown. n.a., not analysed; b.d.l., below detection limit; n.av., not available; MTZ, Moho transition zone; Govin.1994, values from Govindaraju (1994).
*Total Fe given as FeO.
[1]Data from Proenza *et al*. (2006).
[2]Major-element data from Proenza *et al*. (2006) and trace elements analysed here.
[3]Nb and Ta replicate analyses at the Géosciences Montpellier laboratory.
[4]Data from Marchesi *et al*. (2006).

Téneme intrusive, and three cumulate gabbros from the Moa–Baracoa ophiolitic massif.

Mineral concentrates of clinopyroxene and plagioclase were obtained by crushing and sieving (100–200 μm mesh) followed by magnetic separation in a Frantz® isodynamic device. Clean mineral separates were handpicked in alcohol under a binocular microscope. The pervasive presence of fine intergrowths of clinopyroxene and plagioclase made it extremely difficult to obtain optically pure mineral separates. To improve mineral quality, hand-picked separates were ultrasonically washed in diluted 2·5N HCl, kept on a hotplate at about 60°C and rinsed several times with ultrapure water. However, in many samples, the mineral separates still contained mixed grains.

Details on the digestion procedure followed at the Géosciences Montpellier clean room isotopic laboratory have been given by Bosch *et al*. (2004). Pb chemical separation was carried out using AG1X8 anion exchange resin washed in 0·5N HBr and 6N HCl. Nd and Sr were separated following an extraction chromatographic method modified from Pin *et al*. (1994). Average Nd, Sr and Pb concentrations in procedural blanks were less than 30, 70 and 50 pg, respectively.

Pb and Nd isotopic ratios were measured using a P54 Fisons multi-collector (MC)-ICP-MS system or a NuPlasma 500 MC-ICP-MS system at the Ecole Normale Supérieure de Lyon (France). Pb isotope compositions were analysed using the Tl normalization method described by White *et al*. (2000). Each batch of two samples was bracketed by NBS 98l standard splits and an external correction was applied to the samples according to the value reported by Todt *et al*. (1996). The Nd isotopic ratios were measured following the method described by Luais *et al*. (1997); the average value of the Lyon in-house JMC standard solution (batch 801149A) was $0{\cdot}512137 \pm 44$ (2σ) ($n=42$) for four analytical sessions. Sr isotopic ratios were measured by thermal ionization mass spectrometry (TIMS) using a CAMECA TSN 206 system at the Laboratoire Géosciences Azur of the Université de Nice–Sophia Antipolis (France) or a ThermoFinnigan Triton Tl system at the LABOGIS of the Centre Universitaire de Formation et de Recherche de Nîmes (France). The NBS 987 standard was run at the beginning of each analytical session. The average values for NBS 987 were $0{\cdot}710260 \pm 20$ (2σ) ($n=5$) and $0{\cdot}710243 \pm 10$ (2σ) ($n=7$) for Laboratoire Géosciences Azur and LABOGIS, respectively. $^{87}Sr/^{86}Sr$ ratios were corrected for mass discrimination by normalizing to $^{86}Sr/^{88}Sr$ value of 0·1194. The isotopic ratios of the samples were corrected for the *in situ* radioactive decay since 90 Ma (Table 2) according to the ages of crystallization assigned by Iturralde-Vinent *et al*. (2006). Age corrections for mineral separates and

Table 2: Nd, Sr and Pb radiogenic isotope compositions of selected igneous rocks from eastern Cuba

Sample	Material	$^{143}Nd/^{144}Nd$	$^{143}Nd/^{144}Nd$ (90 Ma)	ϵ_{Nd} (90 Ma)	$^{87}Sr/^{86}Sr$	$^{87}Sr/^{86}Sr$ (90 Ma)	$^{206}Pb/^{204}Pb$	$^{206}Pb/^{204}Pb$ (90 Ma)	$^{207}Pb/^{204}Pb$	$^{207}Pb/^{204}Pb$ (90 Ma)	$^{208}Pb/^{204}Pb$	$^{208}Pb/^{204}Pb$ (90 Ma)
Group 1												
Morel volcanics												
M 200	WR	0·513234 ± 8	0·513091	11·1	0·704291 ± 12	0·703971	18·9188 ± 7	18·4128	15·5348 ± 6	15·5103	37·815 ± 2	37·717
M 201	WR	0·513149 ± 8	0·513010	9·5	0·704129 ± 5	0·703802	18·9081 ± 9	18·3714	15·5285 ± 8	15·5026	37·793 ± 2	37·682
Centeno volcanics												
CEN 200	WR	0·513146 ± 4	0·513019	9·7	0·703911 ± 6	0·703836	18·6432 ± 5	18·2494	15·5295 ± 6	15·5105	38·083 ± 2	37·745
CEN 201	WR	0·513163 ± 3	0·513029	9·9	0·704269 ± 6	0·704155	18·5487 ± 12	18·2787	15·5177 ± 10	15·5046	37·861 ± 3	37·724
CEN 202	WR	0·513120 ± 16	0·512990	9·1	0·703596 ± 5	0·703515	18·3156 ± 6	18·1938	15·4949 ± 6	15·4890	37·765 ± 2	37·655
Group 2												
Guamuta dykes												
GUA 200	WR	0·513161 ± 6	0·513021	9·7	0·702926 ± 9	0·702918	18·2856 ± 15	18·1504	15·4693 ± 14	15·4628	37·849 ± 4	37·739
GUA 201	WR	0·513203 ± 8	0·513057	10·4	0·704333 ± 3	0·704324	18·4536 ± 9	18·2512	15·5324 ± 8	15·5226	38·159 ± 2	37·964
GUA 203	WR	0·513161 ± 3	0·513014	9·6	0·702936 ± 11	0·702932	18·3394 ± 10	18·2480	15·6087 ± 9	15·6043	38·345 ± 2	38·254
GUA 205	WR	0·513174 ± 15	0·513031	9·9	0·702951 ± 3	0·702936	18·3850 ± 4	18·2330	15·5264 ± 3	15·5191	38·127 ± 1	37·994
	Cpx	n.a.			n.a.		18·3135 ± 9		15·5301 ± 7		38·047 ± 2	
	Pl	0·513147 ± 17	0·513086	11·0	n.a.		n.a.		n.a.		n.a.	
Loma de la Bandera dykes												
LB 203	WR	0·513170 ± 3	0·513019	9·7	0·703524 ± 4	0·703495	18·3635 ± 7	18·2514	15·5440 ± 7	15·5386	38·156 ± 2	38·051
LB 204	WR	0·513157 ± 16	0·513026	9·8	0·703285 ± 10	0·703262	18·7228 ± 3	18·1738	15·5381 ± 3	15·5116	37·981 ± 1	37·823
	Pl	0·513120 ± 4	0·513025	9·8	n.a.		18·6014 ± 9		15·5261 ± 9		37·909 ± 2	
Group 3, 3T												
Téneme volcanics												
T 201	WR	0·512895 ± 15	0·512776	5·0	0·703720 ± 20	0·703581	18·7568 ± 4	18·4322	15·5633 ± 3	15·5477	38·135 ± 1	37·988
	Cpx	n.a.			n.a.		18·6634 ± 13		15·5542 ± 10		38·075 ± 3	
	Pl	0·512883 ± 53	0·512723	3·9	n.a.		18·5910 ± 8		15·5609 ± 6		38·099 ± 2	
T 202	WR	0·513060 ± 13	0·512944	8·2	0·703790 ± 20	0·703689	18·6816 ± 9	18·5137	15·5814 ± 9	15·5733	38·196 ± 3	38·131
	Cpx	n.a.			n.a.		18·6779 ± 11		15·5747 ± 9		38·165 ± 3	
	Pl	n.a.			n.a.		18·5856 ± 9		15·5830 ± 8		38·197 ± 2	
TEN 1	WR	0·513037 ± 14	0·512951	8·4	0·703890 ± 10	0·703856	18·6196 ± 11	18·4621	15·5643 ± 9	15·5566	38·113 ± 3	38·044
	Cpx	n.a.			0·703660 ± 20	0·703600	n.a.		n.a.		n.a.	
	Pl	0·513084 ± 6	0·513001	9·3	0·704360 ± 10	0·704347	n.a.		n.a.		n.a.	
TM 21	WR	0·513085 ± 17	0·512980	8·9	0·703488 ± 8	0·703391	18·6581 ± 9	18·5180	15·5565 ± 9	15·5497	38·085 ± 3	38·015
	Cpx	0·513133 ± 4	0·512964	8·6	n.a.		n.a.		n.a.		n.a.	
	Pl	0·513108 ± 22			n.a.		n.a.		n.a.		n.a.	

(continued)

Table 2: Continued

Sample	Material	$^{143}Nd/^{144}Nd$	$^{143}Nd/^{144}Nd$ (90 Ma)	ϵ (90 Ma)	$^{87}Sr/^{86}Sr$	$^{87}Sr/^{86}Sr$ (90 Ma)	$^{206}Pb/^{204}Pb$	$^{206}Pb/^{204}Pb$ (90 Ma)	$^{207}Pb/^{204}Pb$	$^{207}Pb/^{204}Pb$ (90 Ma)	$^{208}Pb/^{204}Pb$	$^{208}Pb/^{204}Pb$ (90 Ma)
Téneme boninite												
TM 1	WR	0·513047 ± 11	0·512927	7·9	0·703942 ± 4	0·703901	18·6055 ± 8	18·4278	15·5656 ± 9	15·5570	38·094 ± 3	38·024
	Cpx	0·513125 ± 4	0·512947	8·3	n.a.		18·5371 ± 17		15·5617 ± 12		38·037 ± 4	
Téneme intrusive												
DT 200	WR	0·512767 ± 12	0·512662	2·7	0·705114 ± 4	0·704778	19·0050 ± 8	18·6141	15·6437 ± 9	15·6248	38·691 ± 2	38·387
Estrella de Mayarí dyke												
CAR 4	WR	0·512950 ± 13	0·512855	6·5	0·703620 ± 10	0·703539	18·7296 ± 11	18·5823	15·5702 ± 8	15·5631	38·309 ± 3	38·224
	Cpx	n.a.			0·703580 ± 20	0·703538	n.a.		n.a.		n.a.	
Group 3, 3Q												
Quibiján volcanics (Q1)												
Q 206	WR	0·513031 ± 13	0·512911	7·6	0·704111 ± 4	0·703914	18·7529 ± 4	18·6205	15·5721 ± 4	15·5657	38·202 ± 1	38·129
	Cpx	n.a.			n.a.		18·7528 ± 8		15·5748 ± 7		38·200 ± 2	
Q 208	WR	0·513117 ± 23	0·513002	9·4	0·704255 ± 7	0·704140	18·7766 ± 11	18·5679	15·5688 ± 10	15·5587	38·151 ± 3	38·072
	Cpx	n.a.			0·704025 ± 11	0·703806	n.a.		n.a.		n.a.	
	Pl	0·513084 ± 11			0·704790 ± 10	0·704783	n.a.		n.a.		n.a.	
Quibiján volcanics (Q2)												
Q 202	WR	0·512815 ± 14	0·512693	3·4	0·705440 ± 20	0·705307	18·4113 ± 7	18·2889	15·5953 ± 8	15·5894	38·062 ± 2	38·003
	Cpx	n.a.			n.a.		18·4066 ± 6		15·5933 ± 6		38·041 ± 2	
Q 209	WR	0·512823 ± 13	0·512700	3·5	0·705240 ± 20	0·705020	18·2758 ± 11	18·2429	15·5829 ± 8	15·5813	37·968 ± 3	37·950
	Cpx	n.a.			0·704160 ± 10	0·704097	18·6988 ± 16	18·2556	15·5562 ± 12	15·5348	38·099 ± 3	
	Pl	n.a.			0·705060 ± 10	0·704120	18·2430 ± 15	18·2380	15·5795 ± 11	15·5792	37·947 ± 3	37·943
Q 210	WR	0·512897 ± 13	0·512792	5·3	0·704419 ± 5	0·704355	18·3965 ± 19	18·2715	15·5817 ± 15	15·5757	38·014 ± 4	37·940
	Cpx	0·512958 ± 25	0·512802	5·5	n.a.		18·3103 ± 7		15·5776 ± 7		37·970 ± 2	
Moa–Baracoa ophiolitic gabbros												
Crustal gabbros, Cayo Grande												
CY 200	WR	0·513176 ± 13	0·513011	9·5	0·703240 ± 10	0·703226	18·1626 ± 13	18·1487	15·4857 ± 11	15·4851	37·640 ± 3	37·628
	Cpx	0·513183 ± 5	0·513028	9·8	0·702310 ± 20	0·702246	n.a.		n.a.		n.a.	
Crustal gabbros, Quemado del Negro												
QN 4	WR	0·513248 ± 15	0·513086	11·0	0·702600 ± 10	0·702598	18·1727 ± 11	18·1641	15·4862 ± 10	15·4858	37·641 ± 3	37·635
	Pl	0·513145 ± 37	0·513068	10·6	0·702730 ± 40	0·702726	n.a.		n.a.		n.a.	
Moho transition zone sill, Cayo Guam												
CG 17	WR	0·513052 ± 37	0·512893	7·2	0·702834 ± 10	0·702826	18·1560 ± 14		15·4906 ± 11		37·643 ± 3	37·642
	Cpx	0·513319 ± 4	0·513138	12·0	0·702450 ± 50	0·702405	n.a.		n.a.		n.a.	

Ratios corrected for radioactive decay since 90 Ma are also shown, except for samples with abundances of the parent elements below the detection limits. WR, whole-rock; n.a., not analysed.

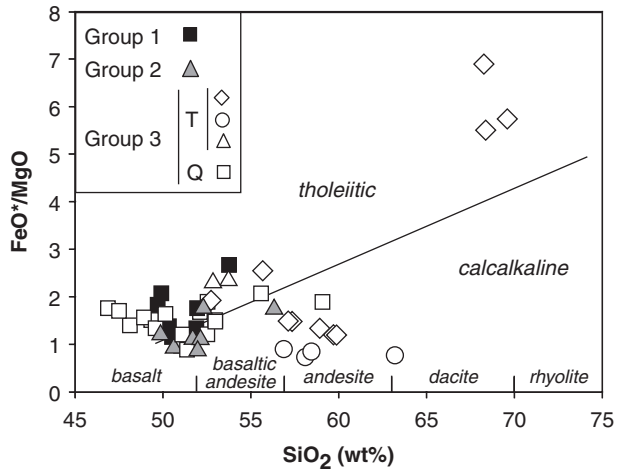

Fig. 2. SiO_2 vs FeO*/MgO for volcanic rocks and dykes from eastern Cuba showing the discriminant boundary between tholeiitic and calcalkaline magmatic suites (Miyashiro, 1974). Data plotted on an anhydrous basis in wt%. FeO* is total Fe as FeO. ■, Group 1 volcanic rocks; ▲, Group 2 dykes. ◇, Téneme volcanic rocks (Group 3T); ○, Téneme boninites (Group 3T); △, Estrella de Mayarí dykes (Group 3T); □, Quibiján volcanic rocks (Group 3Q). One dyke of Group 2 (LB 204) is not plotted because its whole-rock composition reflects significant amphibole accumulation.

whole-rocks were made based on data from laser ablation (LA)-ICP-MS and ICP-MS analyses, respectively; the reproducibility of trace-element analyses does not affect the interpretation of the isotopic data. For samples with Rb, Sm, Th and U contents below the analytical detection limits we present only the present-day age-uncorrected isotopic values; this is the case for the great majority of the Pb isotopic data for mineral separates.

WHOLE-ROCK GEOCHEMISTRY

Major elements

The sampled volcanic rocks and dykes consist of basalts (25), basaltic andesites (15), and minor andesites (8) and dacites (4) (Fig. 2). Secondary alteration processes probably account for some of the scatter in K_2O vs Mg-number [100 × molar MgO/(MgO + FeO*); where FeO* is total Fe] and for the slightly high SiO_2–Na_2O and low CaO contents in several volcanic rocks (not illustrated). On the other hand, the trends of Mg-number vs FeO*, TiO_2 and Al_2O_3 are consistent with the magmatic differentiation within the suites (Fig. 3) and we infer that their abundances have not been significantly affected by alteration.

In terms of whole-rock major-element composition, the igneous rocks from eastern Cuba can be classified into three main magmatic groups that are discriminated by their trends in the Mg-number vs FeO* diagram (Fig. 3a).

Group 1 comprises basalts and rare basaltic andesites from the Morel, La Melba and Centeno areas, which

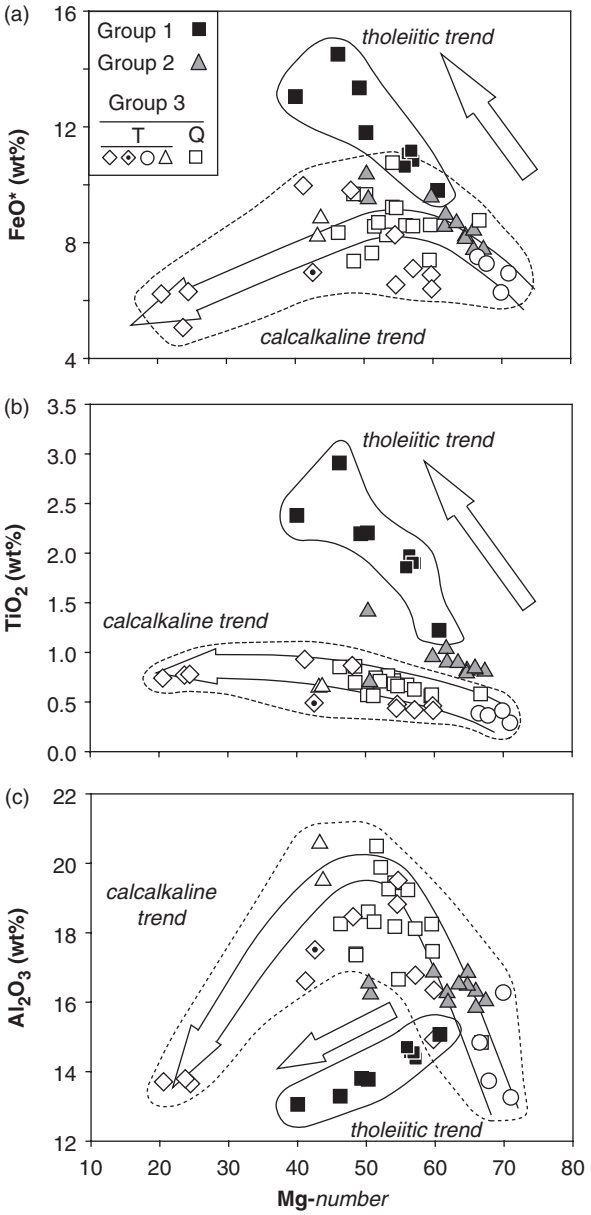

Fig. 3. Whole-rock major-element compositions of igneous rocks from eastern Cuba illustrated by Mg-number vs FeO* (a), TiO_2 (b) and Al_2O_3 (c). Data plotted on an anhydrous basis in wt%. Symbols as in Fig. 2. The Téneme intrusive sample not plotted in Fig. 2 has been included here (open diamond with dot). Tholeiitic and calcalkaline differentiation trends marked by continuous and dashed lines, respectively.

exhibit steady FeO* enrichment with decreasing Mg-number. FeO enrichment during differentiation is commonly ascribed to the tholeiitic line of descent (Miyashiro, 1974).

Group 2 includes dykes from the Guamuta–Loma de la Bandera and Cerrajón areas. They have a basaltic to basaltic andesitic composition. In terms of Mg-number vs FeO*

variations, these samples display a trend similar to that of Group 1 but at slightly lower FeO* for a given Mg-number.

Group 3 includes basaltic to dacitic samples from the Téneme and Quibiján type localities and the Estrella de Mayarí region. These rocks define a calcalkaline evolutionary trend that is characterized by first increasing and then decreasing FeO* with decreasing Mg-number. Within this group, we further distinguish two subgroups: Group 3T, which comprises samples from the Téneme Formation (some of which exhibit a boninitic affinity, with $SiO_2 > 53$ wt%, $TiO_2 < 0{\cdot}5$ wt% and MgO >8 wt%) and the Estrella de Mayarí dykes, and Group 3Q, which includes volcanic rocks of the Quibiján Formation.

Similar evolutionary trends are also observed in the Mg-number vs TiO_2 diagram (Fig. 3b). In Groups 1 and 2, the TiO_2 content increases significantly with differentiation, whereas there is only a weak enrichment trend in Group 3. The relatively high TiO_2 contents of Group 1 volcanic rocks are characteristic of the tholeiitic series from mid-ocean ridges and back-arc basins, whereas the lower TiO_2 abundances of Groups 2 and 3 are distinctive of island arc lavas (e.g. Jakeš & Gill, 1970). In Group 1 plagioclase fractionation results in decreasing Al_2O_3 from the primitive to evolved lavas, whereas Group 2 samples have nearly homogeneous Al_2O_3 contents (Fig. 3c). The delay of the plagioclase fractionation in Group 3 led to Al_2O_3 enrichment in the most primitive samples followed by decreasing Al_2O_3 abundances at Mg-numbers <50.

Trace elements

Chondrite-normalized (after Sun & McDonough, 1989) REE patterns of the analysed samples are illustrated in Fig. 4. Group 1 and 2 rocks have light REE (LREE)-depleted to flat patterns ($La/Yb_{(N)} = 0{\cdot}6$–$0{\cdot}9$) comparable with MORB and IAT. Group 1 exhibits higher REE concentrations than Group 2 and variable negative Eu anomalies, indicative of plagioclase fractionation. The REE contents of Group 2 are similar to those of the Early Cretaceous IAT series from the Caribbean region, represented by the dashed field in Fig. 4.

The REE patterns of Group 3 samples significantly differ from those of Groups 1 and 2. Group 3 rocks display REE patterns characterized by LREE-enriched ($La/Sm_{(N)} = 1{\cdot}0$–$2{\cdot}1$) and HREE-depleted ($Sm/Yb_{(N)} = 1{\cdot}1$–$1{\cdot}8$) segments typical of arc lavas (e.g. McCulloch & Gamble, 1991; Hawkesworth *et al.*, 1993; Kelemen *et al.*, 2003). No appreciable difference exists between the REE patterns of Groups 3T and 3Q. Negative Eu anomalies as a result of plagioclase fractionation are present only in the most evolved lavas with the highest REE contents. The samples of Group 3T with a boninitic affinity display REE patterns ($La/Sm_{(N)} = 1{\cdot}1$–$2{\cdot}4$; $Sm/Yb_{(N)} = 1$–$2{\cdot}4$) similar to those of the other Téneme volcanic rocks but show a wider range of LREE enrichment. LREE and MREE abundances are lower and normalized patterns slightly flatter in Group 3 compared with other Caribbean calcalkaline suites represented by the grey field in Fig. 4.

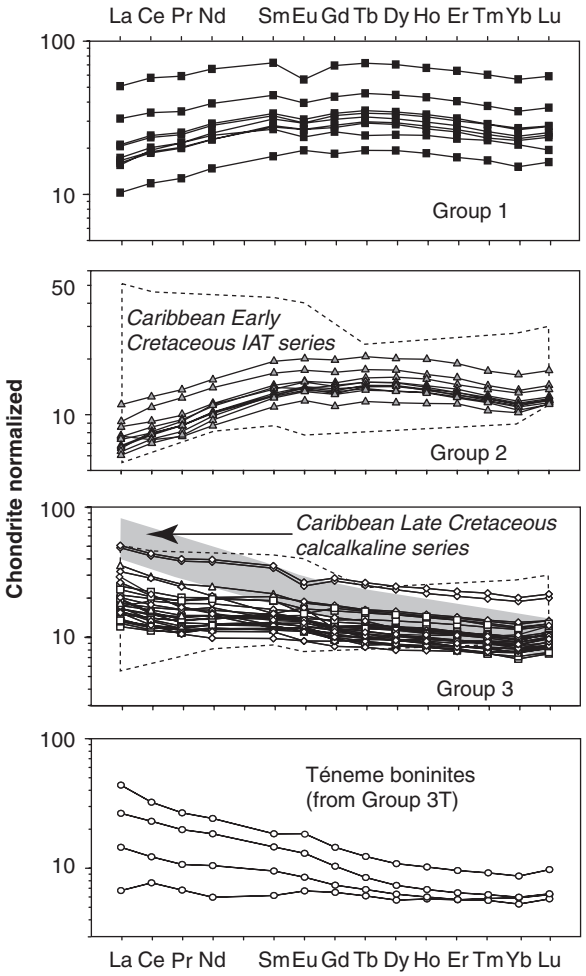

Fig. 4. Chondrite-normalized REE patterns of igneous rocks from eastern Cuba (whole-rock analyses). Symbols as in Fig. 2. Normalizing values from Sun & McDonough (1989). Fields of the Caribbean Early Cretaceous IAT series (dashed line) and Late Cretaceous calcalkaline series (grey area) from Kerr *et al.* (1999) and Blein *et al.* (2003), respectively.

Figure 5 shows that the three groups identified above based on their distinctive major-element and REE signatures also differ significantly in terms of La/Nb and Th/Nb ratios. These ratios vary between oceanic abyssal tholeiites, arc lavas and continental crust (Plank, 2005), thus constituting useful tracers for subduction-related processes and recycled continental material. In Fig. 5 Group 1 samples clearly display MORB-like ratios whereas the dykes of Group 2 have higher La/Nb and Th/Nb. Group 3 samples have significantly higher values of these ratios and overlap the composition of common arc magmas. Th/La is generally greater in subduction-related rocks compared with MORB and is mainly influenced by the composition of

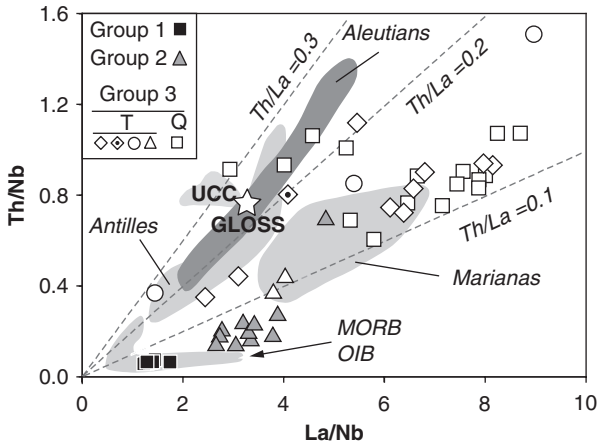

Fig. 5. La/Nb vs Th/Nb for igneous rocks from eastern Cuba (whole-rock analyses). Symbols as in Fig. 3. Fields of MORB–OIB, Marianas, Aleutians, Antilles arcs, upper continental crust (UCC) and global subducting sediment (GLOSS, white star) from Plank (2005) and references therein. One boninitic sample with a high La/Nb ratio has been omitted for clarity.

subducted sediments (Plank, 2005). The majority of Group 3 samples have Th/La <0·15, resembling Marianas arc lavas, whereas three 3Q and one 3T volcanic rocks are characterized by significantly higher Th/La (≥0·23), characteristic of Lesser Antilles and Aleutians arc volcanic rocks.

RADIOGENIC ISOTOPE COMPOSITIONS

Figure 6 illustrates the variation in the Nd, Sr and Pb radiogenic isotope compositions of mineral separates and whole-rocks for the studied samples (see Table 2). The samples of Groups 1 and 2 exhibit high $\epsilon_{Nd\ (90\ Ma)}$ values (9·1–11·1) indicative of a depleted MORB mantle source (DMM) (Workman & Hart, 2005); Group 2 samples commonly have a slightly more depleted signature than Group 1. Three olivine gabbros from the Moa–Baracoa ophiolitic massif have ϵ_{Nd} radiogenic values broadly similar to those of Group 1; this observation is in good agreement with the data of Marchesi *et al.* (2006). Group 3 samples have Nd isotope compositions significantly less radiogenic than those of Groups 1 and 2, consistent with a stronger imprint of a subduction component in these samples; $\epsilon_{Nd\ (90\ Ma)}$ varies from 2·7 to 9·3 in Group 3T and from 3·4 to 9·4 in Group 3Q.

The impossibility of obtaining pure clinopyroxene separates, combined with the pervasive alteration of plagioclase, make it difficult to determine the primary Sr isotopic compositions of our samples. Relatively high $^{87}Sr/^{86}Sr$ ratios decoupled from ϵ_{Nd} decrease are commonly ascribed to seawater alteration. Seawater contamination is particularly evident for Group 1 ($0{\cdot}70351 < {}^{87}Sr/{}^{86}Sr_{(90\ Ma)} < 0{\cdot}70415$) and Group 2

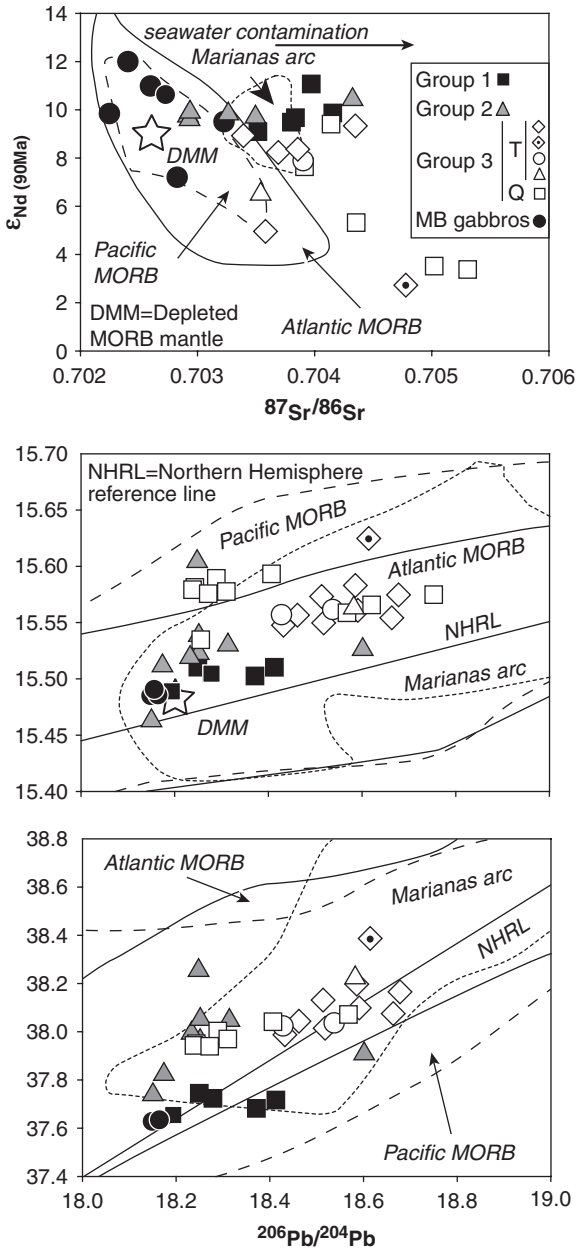

Fig. 6. Nd, Sr and Pb isotope ratios of whole-rocks and mineral separates for igneous rocks from eastern Cuba. For samples with known Rb, Sm, Th and U contents the data have been corrected for time-integrated radioactive decay since 90 Ma, according to the crystallization ages assigned by Iturralde-Vinent *et al.* (2006); otherwise, maximum present-day age-uncorrected values have been plotted. Symbols as in Fig. 3. •, cumulate gabbros from the Moa–Baracoa (MB) ophiolitic massif. Depleted MORB mantle (DMM; star) from Workman & Hart (2005); Atlantic (continuous line) and Pacific (long dashed line) MORB fields from Hofmann (2003) and references therein; Marianas arc volcanic rocks field (short dashed line) from the GEOROC database (http://georoc.mpch-mainz.gwdg.de/georoc/Entry.html); NHRL (Northern Hemisphere reference line) from Hart (1984).

($0{\cdot}70292 < {}^{87}Sr/{}^{86}Sr_{(90\ Ma)} < 0{\cdot}70432$), which depart from the Atlantic and Pacific MORB fields, unlike the Moa–Baracoa ophiolitic gabbros. Group 3 samples have variable $^{87}Sr/^{86}Sr$ ratios that increase from Group 3T ($0{\cdot}70339 < {}^{87}Sr/{}^{86}Sr_{(90\ Ma)} < 0{\cdot}70478$) to Group 3Q ($0{\cdot}70381 < {}^{87}Sr/{}^{86}Sr_{(90\ Ma)} < 0{\cdot}70531$).

Group 1 volcanic rocks exhibit rather variable $^{206}Pb/^{204}Pb_{(90\ Ma)}$ (18·19–18·41) and more constant $^{207}Pb/^{204}Pb_{(90\ Ma)}$ (15·49–15·51) and $^{208}Pb/^{204}Pb_{(90\ Ma)}$ (37·65–37·74) ratios. Group 2 generally has overlapping $^{206}Pb/^{204}Pb_{(90\ Ma)}$, and higher $^{207}Pb/^{204}Pb_{(90\ Ma)}$ (15·46–15·60) and $^{208}Pb/^{204}Pb_{(90\ Ma)}$ (37·74–38·25) ratios compared with Group 1. We note that the high whole-rock U/Pb ratio of one Group 2 dyke (LB 204) leads to an overestimate of the time-integrated U decay since its crystallization; this is reflected by the relatively low age-corrected Pb isotopic ratios of this specimen compared with the other rocks of the suite. We have thus corrected its Pb isotopic composition considering the primary U abundance as the value interpolated between the normalized contents of Th and La (Hofmann, 2003). Group 3 samples have more radiogenic Pb isotopic compositions than Groups 1 and 2 ($^{206}Pb/^{204}Pb_{(90\ Ma)} = 18{\cdot}24–18{\cdot}62$; $^{207}Pb/^{204}Pb_{(90\ Ma)} = 15{\cdot}53–15{\cdot}62$; $^{208}Pb/^{204}Pb_{(90\ Ma)} = 37{\cdot}94–38{\cdot}39$), consistent with a stronger imprint of a subduction component in this group. Group 3Q samples with high Th/La ratios (Fig. 5) cluster at lower $^{206}Pb/^{204}Pb$–$^{208}Pb/^{204}Pb$ and have higher $^{207}Pb/^{204}Pb$ ratios than other Group 3 volcanic rocks. The dispersion of mineral and whole-rock data observed for some samples (Table 2, Fig. 6) is due to the fact that most mineral Pb isotopic data reported in our study are present-day ratios and are, therefore, considered as maximum values. The Pb isotope ratios of whole-rock analyses, on the other hand, are age-corrected. For this reason, in the following discussion we will use only the age-corrected data for whole-rocks, and focus particularly on their Pb isotopic variations, which are significantly less affected by seawater alteration than Sr isotopes (e.g. Schaule & Patterson, 1981).

DISCUSSION

Trace-element and radiogenic isotope data indicate that the Cretaceous magmatism in eastern Cuba can be classified into three main igneous groups, with different imprints of a subduction component. Group 1 is composed of basalts and rare basaltic andesites with MORB-like geochemical affinity, which could have formed in either a mid-ocean or back-arc spreading centre. Group 2 comprises basaltic and minor basaltic andesitic dykes with transitional compositions between Groups 1 and 3, and that have IAT signatures probably reflecting the onset of arc growth (Jakeš & Gill, 1970), arc rifting (Gribble *et al.*, 1998), or back-arc volcanism close to the arc front (Taylor & Martinez, 2003). Group 3 consists of volcanic and minor intrusive rocks that have an unambiguous subduction-related imprint indicating an origin in the proximity of the volcanic arc. As Group 2 and some Group 3T samples are dykes intrusive into residual mantle peridotite, their imprinting by a subduction component is not due to assimilation of arc crust but must be related to the subducting slab.

Discriminating between these tectonic scenarios and establishing potential genetic links between the magmatic groups requires deciphering which geochemical signatures come from the mantle wedge and/or back-arc mantle and which are derived from the subducted slab (e.g. Hawkesworth *et al.*, 1991, 1993; McCulloch & Gamble, 1991; Pearce & Peate, 1995). Below we use trace elements and radiogenic isotope ratios to examine the depletion and melting extents of the mantle source, assess the relative contributions of the mantle and the slab in the magma source, and identify the nature of the slab component for each magmatic group distinguished. These results are then compared with data for Cretaceous arc magmatism in the Caribbean region to infer how they can be integrated into the differing geodynamic models proposed.

Extent and depth of melting of the mantle source

Absolute abundances of HREE and HFSE and selected ratios between these elements are commonly employed as proxies of mantle wedge composition and for estimating the degree of melting in island arc settings, because these elements are least affected by the introduction of a slab component (Pearce, 1983; McCulloch & Gamble, 1991; Pearce & Parkinson, 1993; Woodhead *et al.*, 1993; Pearce & Peate, 1995). To minimize the effects of fractional crystallization and crustal contamination, estimations of source heterogeneity and melting proportions are inferred based on the HFSE and HREE abundances of basaltic rocks with Mg-number >50 and $SiO_2 < 53$ wt%. As a consequence, samples of Group 3T were excluded.

The extent of incompatible element depletion and depth of melting are indicated in Fig. 7, which illustrates the correlation between Lu and Dy in primitive igneous rocks from eastern Cuba together with non-modal batch melting models for spinel lherzolite and garnet lherzolite mantle sources. Because Lu is fractionated from Dy during garnet-present melting, melting trends in the presence of spinel and garnet have different slopes. The Lu–Dy variations of Group 1 samples are consistent with <5 to 15% melting of a moderately depleted spinel lherzolite source. The lower HREE contents of Group 2 samples could be related to higher degrees of melting (20–30%) of the same source, or to smaller degrees of melting of a more depleted source. The lowest HREE abundances in Group 3Q samples suggest that they were generated by 10–25% melting of a depleted spinel lherzolite source. Because Lu and Dy abundances are not corrected for fractionation,

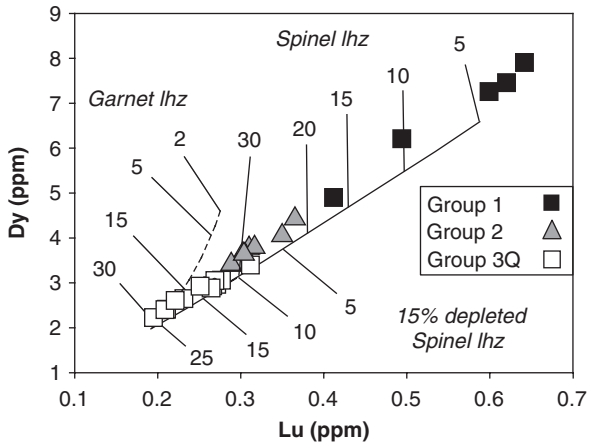

Fig. 7. Lu vs Dy (ppm) for primitive volcanic rocks (Mg-number >50; SiO_2 <53 wt%) from eastern Cuba (whole-rock analyses). Symbols as in Fig. 2. Non-modal batch melting curves are labelled for variable melting degrees of spinel lherzolite (lhz) (continuous line) [source and melting ol:opx:cpx proportions 0·57:0·28:0·15 and –0·13:–0·27:1·4, respectively (Walter *et al.*, 1995)] and garnet lherzolite (dashed line) [source and melting ol:opx:cpx:grt proportions 0·52:0·29:0·16:0·03 and 0:0·45:0·45:0·1, respectively (Gribble *et al.*, 1998)] with depleted composition (Donnelly *et al.*, 2004). Partition coefficients from Bedini & Bodinier (1999), Su & Langmuir (2003) and Donnelly *et al.* (2004).

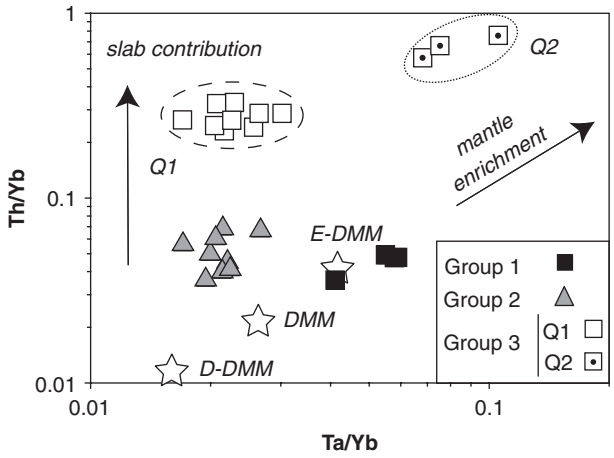

Fig. 8. Ta/Yb vs Th/Yb plot for primitive volcanic rocks from eastern Cuba (whole-rock analyses). Symbols as in Fig. 2. Open squares with dot, Quibiján 2 (Q2) volcanic rocks. DMM, D-DMM and E-DMM (stars) from Workman & Hart (2005). D, depleted; E, enriched.

the estimated melting proportions represent minimum values. The results indicate that melting occurred mainly at spinel lherzolite facies depths, which constrains the maximum pressure of melting to ~2·5 GPa (Walter, 2003) corresponding to depths of about 85 km. These estimates of maximum melting depths are similar to those inferred for coeval arc volcanism in Puerto Rico (Jolly *et al.*, 2001) and probably imply a steady slab dip for the Cretaceous Greater Antilles subduction system.

If the HFSE contents of the mantle source are unmodified by slab additions and melting occurs at moderate to high degrees in the absence of residual garnet—as proposed in the case of our samples (Fig. 7)—Ta/Yb variations should highlight the relative depletion of the mantle source (Pearce, 1983; Pearce *et al.*, 2005). On the other hand, slab additions will increase Th/Yb in volcanic rocks relative to the trend defined by variably depleted MORB mantle sources (Pearce & Peate, 1995). Figure 8 shows the Ta/Yb vs Th/Yb systematics of the most primitive samples (i.e. those with Mg-number >50 and SiO_2 <53 wt%) of each magmatic group distinguished here. Groups 1 and 2 have a limited within-group Ta/Yb variation, whereas values are bimodal in Group 3Q. The mantle source of Group 1 has Ta/Yb close to the enriched-DMM (E-DMM; Fig. 8) (Workman & Hart, 2005) and is markedly less depleted than the source of Group 2, which is characterized by Ta/Yb between the depleted-DMM (D-DDM; Fig. 8) and the average DMM (DMM; Fig. 8) end-members. The relative depletion of Group 2 is accompanied by a departure from the MORB-mantle trend as a result of higher Th/Yb for a given Ta/Yb. In active subduction settings, a similar relative depletion of the mantle source is commonly observed between back-arc (less-depleted source) and arc basalts (more depleted source) (Ryerson & Watson, 1987; McCulloch & Gamble, 1991; Woodhead *et al.*, 1993). This feature is interpreted as evidence that arc basalts record remelting of the back-arc mantle coupled with the introduction of the slab component beneath the magmatic arc (Davidson, 1987; Ewart & Hawkesworth, 1987; McCulloch & Gamble, 1991; Pearce & Parkinson, 1993; Arculus, 1994). Ta/Yb reveals that most of the primitive Group 3Q rocks have a highly depleted source composition similar to that of Group 2 (Fig. 8), whereas three samples have higher Ta/Yb indicative of a relatively more enriched mantle source. These Group 3Q subgroups are referred to hereafter as Groups 3Q1 and 3Q2, respectively (Fig. 8). As Group 3Q samples are from the same volcanic sequence, their Ta/Yb bimodality reflects considerable local variation in the depletion of the mantle source.

Fractionation of HFSE: distinguishing between mantle wedge and slab contributions

If the HFSE budget is dominated by the mantle wedge component and unmodified by slab contributions, the ratios of HFSE with similar mantle–melt partition coefficients, such as Nb/Ta and Zr/Hf, serve as further proxies of the relative degrees of depletion and melting of the sub-arc mantle (Plank & White, 1995; Eggins *et al.*, 1997; Elliott *et al.*, 1997). The Nb/Ta and Zr/Hf ratios of mantle-derived basalts are slightly fractionated during partial melting of mantle peridotite as a result of the more incompatible

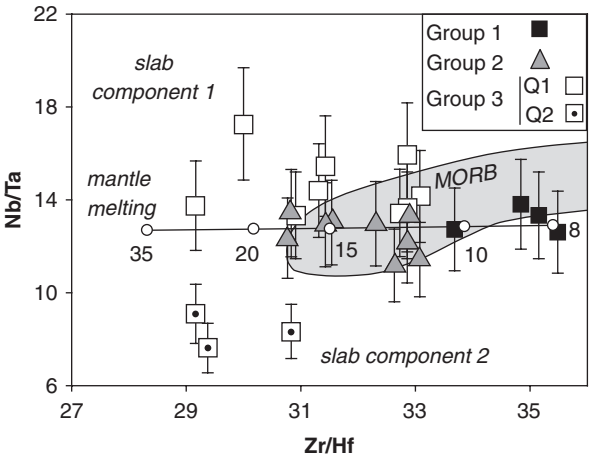

Fig. 9. Zr/Hf vs Nb/Ta plot for primitive volcanic rocks from eastern Cuba (whole-rock analyses). Symbols as in Fig. 8. MORB field (grey shaded area) from Münker *et al.* (2004) and references therein. Non-modal batch melting line is labelled with melting degrees of spinel lherzolite (melting parameters as in Fig. 7) with DMM composition (Workman & Hart, 2005). Nb/Ta initial ratio of the source chosen according to the best fit of the data. Vertical bars represent 14% analytical error in Nb/Ta ratios.

character of the numerators in clinopyroxene (Green *et al.*, 1989; Forsythe *et al.*, 1994).

Figure 9 illustrates the Zr/Hf vs Nb/Ta variations in the most primitive samples (Mg-number >50 and SiO_2 <53 wt%.) Groups 1 and 2 have subchondritic Nb/Ta. Group 2 samples have lower Zr/Hf than Group 1, which, as inferred from the Ta/Yb vs Th/Yb variations (Fig. 8), is consistent with Group 2 samples being derived from a more depleted mantle source than Group 1. The variation of Nb/Ta in Group 3Q is bimodal (Fig. 9), as already noted for Ta/Yb. Group 3Q1 basalts depart from the melting trend defined by the Group 1 and 2 samples in Fig. 9 and have relatively higher and rather variable Nb/Ta (13·3–17·3). Zr/Hf (29·2–33·1) in these rocks has comparable or lower values compared with Group 2. Group 3Q2 primitive samples depart from the MORB field and the melting trend by showing unusually low, subchondritic, Nb/Ta ratios (7·6–9·1) (Fig. 9). The variations of Nb/Ta in Group 3Q samples are inconsistent with anhydrous melting of a peridotite source. Nb and Ta can be fractionated by low degrees of melting, but, as we have shown above (Fig. 7), this is not the case for Group 3Q. Hydrous mantle melting in the presence of high-Mg-number amphibole cannot explain the HFSE fractionation of Group 3Q samples, because this process does not fractionate Nb from Ta (Tiepolo *et al.*, 2000; Foley *et al.*, 2002). Pre-existing carbonate metasomatism of the mantle source might account for the higher Nb/Ta of Group 3Q1 (Green, 1995), but this process should also induce high Zr/Hf ratios (Dupuy *et al.*, 1992), which are very different from the relatively low values observed in this group (Fig. 9).

The HFSE distribution in the Group 3Q samples is inconsistent with a mantle wedge origin of the observed HFSE fractionations and suggests instead that they were imposed by a slab component (e.g. Stolz *et al.*, 1996; Münker, 1998; Prouteau *et al.*, 2000; Foley *et al.*, 2002; Münker *et al.*, 2004; Gómez-Tuena *et al.*, 2007). If so, the bimodal distribution of Ta/Yb values in Group 3Q (Fig. 8) cannot be interpreted in terms of a variably depleted sub-arc mantle source. Most probably, the Group 3Q arc volcanic rocks shared a highly depleted mantle source, as attested by their Lu–Dy variations (Fig. 7); the systematic variations in their Ta/Yb and Nb/Ta ratios are most readily explained by slab additions of two distinct subduction components as discussed below.

Identification of the slab components

Assessment of trace-element slab additions

Interestingly, the primitive samples of Groups 3Q1 and 3Q2, which we have discriminated previously in terms of their bimodal Ta/Yb–Th/Yb (Fig. 8) and Zr/Hf–Nb/Ta (Fig. 9) systematics, also show distinct Th/La vs $^{206}Pb/^{204}Pb_{(90\ Ma)}$ (Fig. 10a) and $\epsilon_{Nd\ (90\ Ma)}$ (Fig. 10b) variations. These signatures support the imprint of two discrete slab components, which have higher $^{206}Pb/^{204}Pb$ and ϵ_{Nd} and lower Th/La in Group 3Q1 compared with Group 3Q2 (Fig. 10a and b).

The fact that Groups 3Q1 and 3Q2 show two distinct slab contributions coupled with contrasting Ta/Yb and Nb/Ta ratios (Fig. 10c) indicates that their Nb–Ta abundances provide fingerprints that reflect the contribution of the subduction component. Group 3Q2 samples have highly subchondritic Nb/Ta and relatively high Nb/La ratios that cannot be easily explained by fractionation related to slab dehydration or melting, as this signature is inconsistent with the HFSE partition coefficients of common slab mineral assemblages (Foley *et al.*, 2002; Münker *et al.*, 2004, and references therein). This indicates that the Nb/Ta ratios of Group 3Q2 samples were inherited from their slab source. As the HFSE are more easily dissolved in hydrous melts than in aqueous fluids (e.g. Tatsumi *et al.*, 1986; Brenan *et al.*, 1995; Keppler, 1996; Kogiso *et al.*, 1997; Kessel *et al.*, 2005) the slab agent that imposed its Nb/Ta signature on the mantle source of Group 3Q2 was probably a melt. On the other hand, the higher Nb/Ta ratios of Group 3Q1 (Fig. 9) could be generated by fractionation during melting of rutile-bearing eclogite-facies metabasalts (Klemme *et al.*, 2002, 2005; Münker *et al.*, 2004).

In the Th/La vs Nb/Ta diagram (Fig. 11) Group 3Q2 primitive samples have relatively high Th/La and low Nb/Ta plotting in the field of the upper continental crust (UCC) (Kalfoun, 2002, and references therein). This indicates that Nb/Ta in this group was probably inherited from subducted continental sediments. On the other hand,

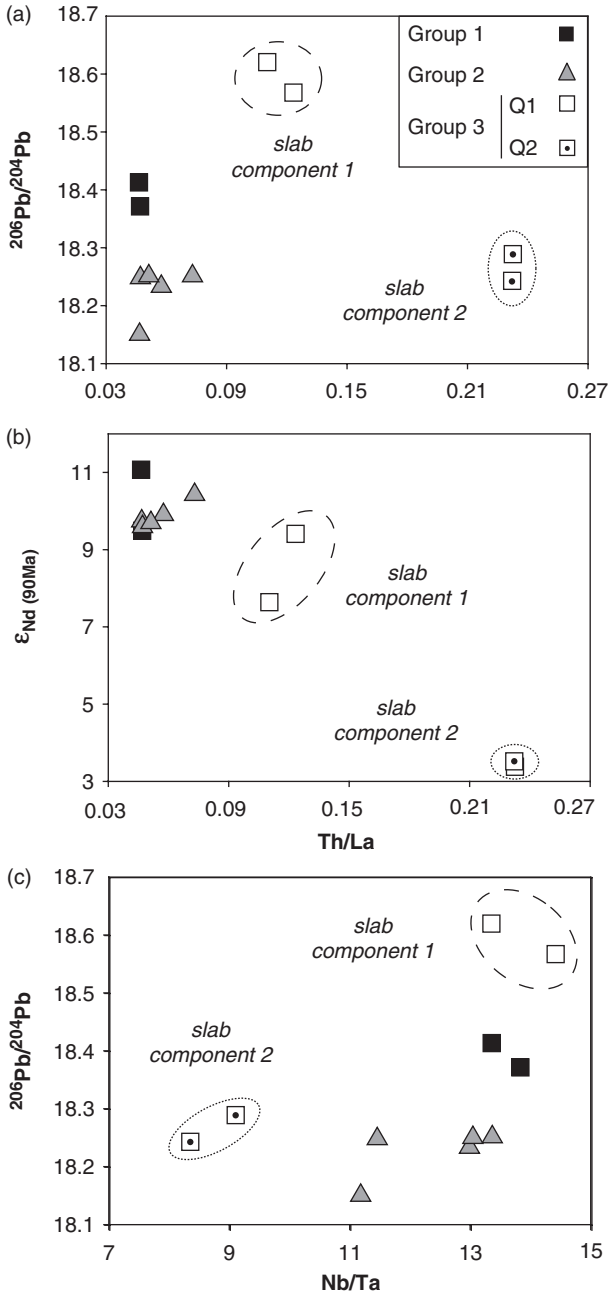

Fig. 10. Th/La vs initial $^{206}Pb/^{204}Pb$ (a) and ϵ_{Nd} (b) and Nb/Ta vs initial $^{206}Pb/^{204}Pb$ (c) for primitive volcanic rocks from eastern Cuba (whole-rock analyses). Symbols as in Fig. 8.

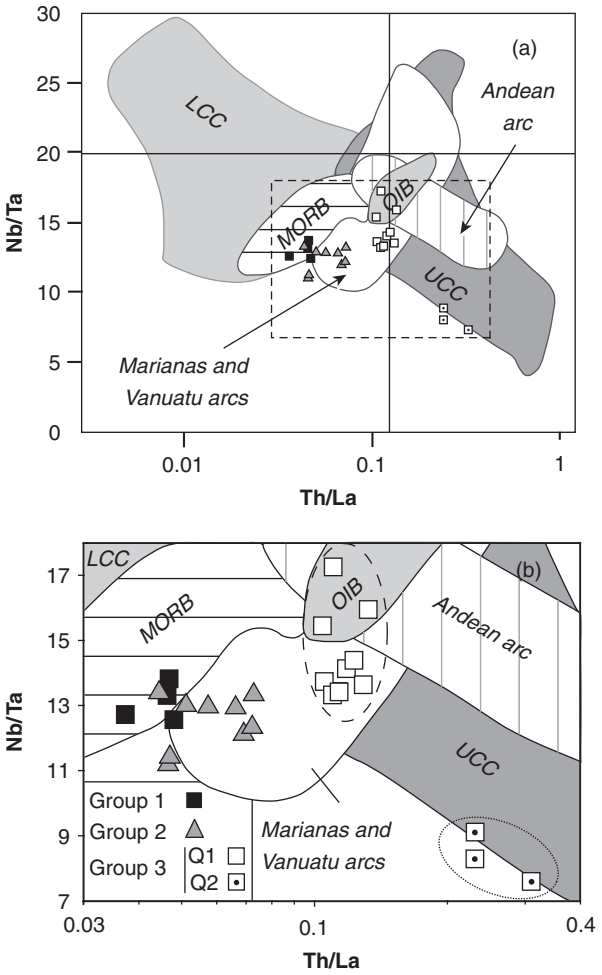

Fig. 11. Th/La vs Nb/Ta for primitive volcanic rocks from eastern Cuba (whole-rock analyses). Symbols as in Fig. 8. Fields of lower and upper continental crust (LCC and UCC, respectively), MORB, OIB, Marianas and Vanuatu arcs, and Andean arc from Kalfoun (2002) and references therein. The crossed lines in (a) mark the chondritic composition (Sun & McDonough, 1989; Münker *et al.*, 2003); the dashed box defines the enlarged area in (b).

the primitive samples of Groups 2 and 3Ql have values similar to those observed in the lavas from the Marianas and Vanuatu island arcs, which are only slightly influenced by recycling of continental sediments (Plank, 2005). We thus infer that the mantle source of Group 3Q2 volcanic rocks received a larger contribution from continental sediments than Group 3Ql, a suggestion that is also supported by their comparatively higher La/Sm ratios (Elliott, 2003). A contribution from continental sediments in the subduction component of Group 3Q2 may also account for the more enriched composition of these rocks in several highly incompatible trace elements (Th–U–Nb–Ta–Pb) corrected for fractionation relative to Group 3Ql (not shown).

The primitive samples of Group 1 plot near the high Th/La side of the MORB field in Fig. 11 consistent with a faint signature of a slab component coherent with a back-arc tectonic setting.

Tracking the nature and provenance of the slab components

Insight into the nature and provenance of the slab component can be obtained from variations in Pb isotope composition, which is a sensitive tracer of slab additions

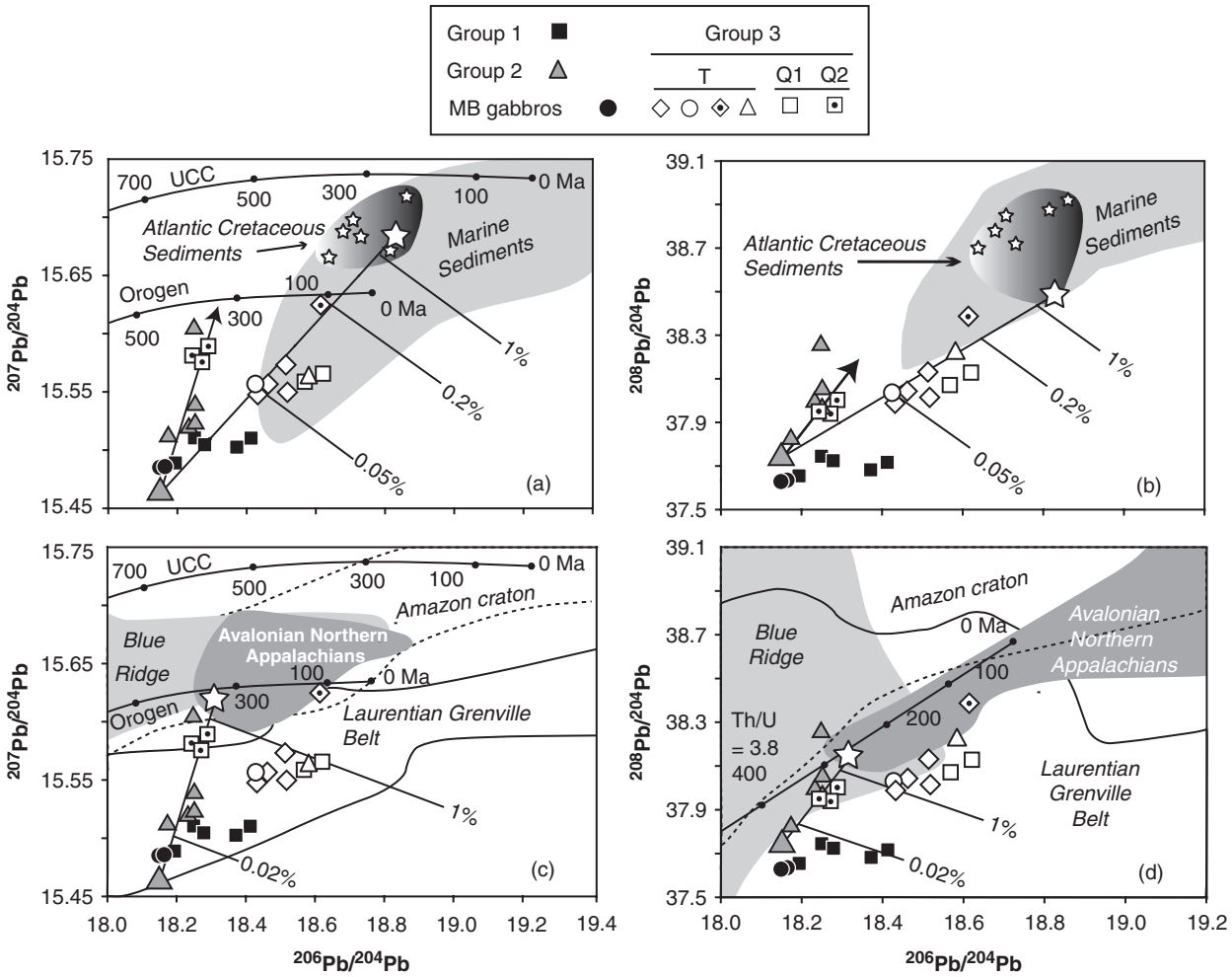

Fig. 12. Whole-rock Pb isotope compositions of igneous rocks from eastern Cuba corrected for radiogenic ingrowth since 90 Ma. Symbols as in Figs 6 and 8. Light grey field of modern marine sediments in (a) and (b) from Ben Othman *et al.* (1989), Elliott *et al.* (1997) and Plank & Langmuir (1998); age-corrected ratios for Atlantic Cretaceous pelagic sediments (stars) from Jolly *et al.* (2006) and references therein; orogen and upper continental crust (UCC) curves from Doe & Zartman (1979). Fields of present-day ratios for the Laurentian Grenville Belt (continuous line), Blue Ridge Terrane and Amazon Craton (dashed line) in (c) and (d) from Tohver *et al.* (2004) and references therein; shaded area of the Avalonian Northern Appalachians continental crust from Ayuso & Bevier (1991). Pb isotopic growth line for average Th/U = 3·8 in (d) from Stacey & Kramers (1975). Mixing lines between the compositions of the assumed mantle wedge (largest grey triangle) and those of one Atlantic Cretaceous sediment and the Appalachians continental crust best fitting with the data (large stars) are shown.

(e.g. Hawkesworth, 1982; Weaver *et al.*, 1986; Hawkesworth *et al.*, 1993; Santos *et al.*, 2002; Elliott, 2003). One sample of Group 2 (GUA 200) is the best candidate to approximate the starting isotope composition of the mantle wedge prior to slab addition, as it plots along the NHRL in the $^{206}Pb/^{204}Pb$ vs $^{207}Pb/^{204}Pb$ diagram (Fig. 6), and has high $\epsilon_{Nd\ (90\ Ma)}$ and the least radiogenic Pb and Sr isotopic ratios among the samples of Groups 2 and 3.

In Pb isotopic diagrams (Fig. 12), samples of Groups 2 and 3 define two distinct trends diverging from the pre-subduction composition of the mantle wedge represented by sample GUA 200. Groups 2 and 3Q2 define a steep trend characterized by relatively low $^{206}Pb/^{204}Pb$ (18·17–18·29) and fairly variable $^{207}Pb/^{204}Pb$ (15·51–15·60) and $^{208}Pb/^{204}Pb$ (37·82–38·25), whereas the rest of the samples (including Groups 3Q1 and 3T) cluster at higher $^{206}Pb/^{204}Pb$ (18·43–18·62). The isotopic composition of Groups 3Q1 and 3T is consistent with mixing of the pre-subduction mantle with marine sediments (Fig. 12a and b), particularly with small percentages (0·05–0·2%) of Cretaceous Atlantic pelagic sediments (Jolly *et al.*, 2006, and references therein). On the other hand, rocks of Groups 2 and 3Q2 scatter towards less radiogenic $^{206}Pb/^{204}Pb$ compositions than marine sediments. In particular, they point toward lower $^{206}Pb/^{204}Pb$ values than those predicted for the arc (Orogen) and upper continental crust (UCC) at 100 Ma (the approximate time of eastern Cuba magmatism) in the model of

Doe & Zartman (1979) (Fig. 12c). We also remark that the $^{208}Pb/^{204}Pb$ of Groups 2 and 3Q2 can be explained by mixing with an end-member characterized by a time-integrated Th/U lower than 3·8 [the average value of the Earth in the two-stage model of Stacey & Kramers (1975)] (Fig. 12d). These features indicate that the continental component involved in the genesis of these magmatic groups was derived from relatively depleted continental crust with rather low time-integrated U/Pb and Th/U.

Taking into account the paleogeography of the Caribbean realm in the Late Cretaceous (Meschede & Frisch, 1998; Pindell *et al.*, 2006), the North and South America cratons are the two most likely sources of continental material entering the western Greater Antilles subduction zone. Relatively low U/Pb and Th/U ratios are characteristic of North American terranes and are significantly different from the signature of the Amazon craton (Tohver *et al.*, 2004). Among the potential candidates for the provenance of these continental sediments, the Avalonian continental crust and the Blue Ridge terrane of the Appalachians range most closely fit the Pb isotopic composition inferred for the continental mixing end-member involved in the genesis of Groups 2 and 3Q2 (Fig. 12c and d). These areas exhibit $^{207}Pb/^{204}Pb$ ratios intermediate between those of the Laurentian Grenville Belt and the Amazon craton (Ayuso & Bevier, 1991; Tohver *et al.*, 2004) and are interpreted as exotic peri-Gondwanan continental terranes derived from South American Proterozoic crust subsequently incorporated into North America (Nance & Murphy, 1994). A similar tectonic evolution has been inferred for the Northern Florida, Yucatán and Chortis blocks (Murphy *et al.*, 2004, and references therein), which were located relatively close to the Cuban arc in the Late Cretaceous (e.g. Pindell *et al.*, 2006). The Pb isotopic systematics of Groups 2 and 3Q2 is consistent with contamination of the mantle wedge by small percentages (<1%) of a slab agent extracted from detrital sediments derived from the North American exotic continental crust in the Appalachians (Fig. 12c and d).

Implications for the geodynamic evolution of the Cretaceous Greater Antilles subduction zone

The compositional variation observed in the eastern Cuba magmatism may be used to discriminate between different potential spatial and/or temporal scenarios for its genesis. For instance, the increasing imprint of a slab component from Group 1 to Groups 2 and 3 may reflect an increasing proximity to the arc volcanic front. In active subduction settings, similar variations are observed both across strike (e.g. Hochstaedter *et al.*, 2001; Sinton *et al.*, 2003) or along strike in a back-arc basin converging on the arc, as is the case of the Marianas subduction zone (Pearce *et al.*, 2005). In the former scenario the stronger contribution from the slab is generally coupled with relatively greater depletion of the mantle source, whereas in the latter scenario there is little or no variation in the source depletion as a function of the distance from the arc axis (Pearce *et al.*, 2005). As the mantle sources of Groups 2 and 3 not only show a progressively stronger imprint of a slab component(s) but also are significantly more depleted than Group 1 (Figs 7–9), we conclude that the geochemical variability of the igneous suites from eastern Cuba probably reflects across-arc variation as indicated in Fig. 13. We also note that this tectonic configuration fits with the genetic relationships between the Mayarí–Baracoa ophiolitic gabbros and the volcanic rocks from eastern Cuba (Marchesi *et al.*, 2006).

The polarity of subduction below the Late Cretaceous Greater Antilles Arc and consequently the age (Aptian vs Campanian) of a hypothetical reversal from a NE- to SW-dipping slab in this arc system are controversial (Kerr *et al.*, 1999, 2003; Jolly *et al.*, 2001; Pindell *et al.*, 2006, and references therein). The geochemical evidence provided in this study of the involvement of North American continental sediments in the genesis of eastern Cuba magmatism (Fig. 12c and d) implies SW subduction of the Proto-Caribbean ocean beneath the Caribbean plate during the Late Cretaceous (Fig. 13). Moreover, the pre-Campanian age of the eastern Cuba igneous suites supports models that establish the onset of SW-dipping subduction beneath the Greater Antilles Arc in the Aptian (García-Casco *et al.*, 2006; Pindell *et al.*, 2006). The involvement of continental sediments in the Cretaceous Greater Antilles subduction zone has been previously suggested by several workers (e.g. Kerr *et al.*, 1999, and references therein) but so far has not been verified in the eastern domain of the paleo-island arc (Hispaniola, Puerto Rico, Virgin Islands), which generally shows a major contribution of marine pelagic sediments (e.g. Lebron & Perfit, 1994; Jolly *et al.*, 2001, 2006). Our results confirm that the Late Cretaceous Cuban arc was located in a setting relatively close to North America (Pindell, 1994; Meschede & Frisch, 1998) where detrital sediments from the paleo-north American continental margin were subducted into the Greater Antilles paleo-subduction zone.

CONCLUSIONS

The Late Cretaceous igneous rocks from eastern Cuba show three main geochemical signatures that mostly reflect the different extent of depletion and the variable imprint of a subduction component in their mantle sources. Group 1 consists of tholeiitic basalts formed by low to moderate degrees of melting (<5–15%) of a depleted mantle source. These rocks exhibit MORB-like compositions with a faint slab-derived component, consistent with a back-arc basin setting. Group 2 was derived by similar degrees of melting of a more depleted mantle source that was overprinted by a significant subduction component.

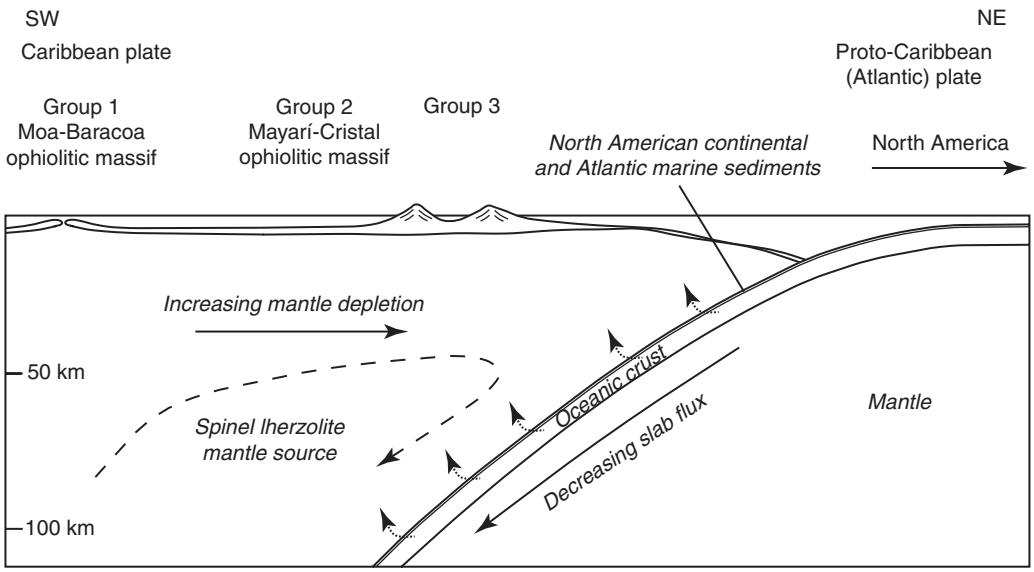

Fig. 13. Proposed tectonic configuration of eastern Cuba in the Late Cretaceous (pre-Campanian) with the inferred settings of the igneous suites studied here. The dashed arrow symbolizes the hypothetical flow trajectory of the mantle in the subduction zone. Short dotted arrows represent the flux of fluid or melt from the subducting slab to the mantle wedge.

The source of Group 3 basalts underwent moderate to high degrees of melting (10–25%) and had a highly depleted composition coupled with a strong subduction-related imprint. The absence of fractionation between MREE and HREE in the primitive basalts indicates that melting mainly occurred at depths (<85 km) characteristic of the spinel lherzolite stability field. Contrary to previous ideas, the Morel (Group 1) and Quibiján (Group 3Q) extrusives record two distinct volcanic settings and are considered as different series. On the other hand, the volcanic suites so far distinguished in the Téneme (Group 3T) and Quibiján (Group 3Q) Formations should be grouped on the basis of their similar whole-rock compositions.

Unlike the samples of Groups 1 and 2, our data indicate that Nb/Ta in the primitive lavas of Group 3 is not controlled by the mantle component, but instead provides a fingerprint of the contributions of two different slab-derived agents: in one case (Group 3Q1) the melting of rutile-bearing subducted crust caused the fractionation of Nb from Ta; in the other case (Group 3Q2) Nb/Ta was inherited from recycled continental sediments.

Both North American continental and Atlantic marine deposits entered the Cuban paleo-subduction zone and mixed in small percentages (<1%) with the depleted mantle sources of Groups 2 and 3Q2, and Groups 3T and 3Q1, respectively. The involvement of North American and Atlantic sediments in the sources of Late Cretaceous magmatism of eastern Cuba indicates that the Proto-Caribbean (Proto-Atlantic) lithosphere subducted beneath the Greater Antilles Arc prior to the Campanian.

The variable depletion and influence of a subduction component in the subarc mantle implicate temporal and/or spatial compositional variations more complex than previously considered for Cretaceous magmatism in eastern Cuba, and may reflect the variable across-arc tectonic settings of the magmatic activity.

ACKNOWLEDGEMENTS

The authors are grateful to J. Blanco-Moreno, R. Díaz-Martínez, J. Batista-Rodríguez and S. Pereira for field assistance. We acknowledge J.-L. Bodinier, O. Bruguier, B. Dhuime and B. Galland (Géosciences Montpellier) for their kind assistance during ICP-MS analyses and chemical separation in the laboratory. We are also grateful to U. Schärer for his great help during Sr isotopic analyses at the Géosciences Azur laboratory, and to J. López Ruiz, J. I. Gil Ibarguchi and J. Lewis for fruitful discussions on the interpretation of the data. Detailed and critical reviews by W. T. Jolly, C. Münker and O. Nebel significantly improved the manuscript. This research has been financially supported by the Spanish Ministerio de Educación y Ciencia (MEC) through research grants BTE2001-3308, CGL2004-00622, and Acciones Integradas Hispano-Francesas HF2002-0093 and HF2005-0066, and by the Junta de Andalucía Research Group RNM 131. C.J.G.'s research has been supported by a Ramón y Cajal fellowship and C.M.'s by a MEC-FPI fellowship.

REFERENCES

Arculus, R. J. (1994). Aspects of magma genesis in arcs. *Lithos* **33**, 189–208.

Ayuso, R. A. & Bevier, M. (1991). Regional differences in Pb isotopic compositions of feldspars in plutonic rocks of the Northern

Appalachian Mountains, U.S.A. and Canada: a geochemical method of terrane correlation. *Tectonics* **10**, 191–312.

Bedini, R. M. & Bodinier, J. L. (1999). Distribution of incompatible trace elements between the constituents of spinel peridotite xenoliths: ICP-MS data from the East African Rift. *Geochimica et Cosmochimica Acta* **63**, 3883–3900.

Ben Othman, D., White, W. M. & Patchett, J. (1989). The geochemistry of marine sediments, island arc magma genesis, and crust–mantle recycling. *Earth and Planetary Science Letters* **94**, 1–21.

Blein, O., Guillot, S., Lapierre, H., Mercier de Lépinay, B., Lardeaux, J. M., Millan Trujillo, G., Campos, M. & Garcia, A. (2003). Geochemistry of the Mabujina Complex, central Cuba: implications on the Cuban Cretaceous arc rocks. *Journal of Geology* **111**, 89–101.

Bosch, D., Jamais, M., Boudier, F., Nicolas, A., Dautria, J.-M. & Agrinier, P. (2004). Deep and high-temperature hydrothermal circulation in the Oman Ophiolite—petrological and isotopic evidence. *Journal of Petrology* **45**, 1181–1208.

Brenan, J., Shaw, H. F., Ryerson, F. J. & Phinney, D. L. (1995). Mineral–aqueous fluid partitioning of trace elements at 900°C and 2·0 GPa: Constraints on the trace element chemistry of mantle and deep crustal fluids. *Geochimica et Cosmochimica Acta* **59**, 3331–3350.

Davidson, J. P. (1987). Crustal contamination versus subduction zone enrichment: Examples from the Lesser Antilles and implications for mantle source compositions of island arc volcanic rocks. *Geochimica et Cosmochimica Acta* **51**, 2185–2198.

Doe, B. R. & Zartman, R. E. (1979). Plumbotectonics, the Phanerozoic. In: Barnes, H. (ed.) *Geochemistry of Hydrothermal Ore Deposits*. New York: Wiley–Interscience, pp. 22–70.

Donnelly, K. E., Goldstein, S. L., Langmuir, C. H. & Spiegelman, M. (2004). Origin of enriched ocean ridge basalts and implications for mantle dynamics. *Earth and Planetary Science Letters* **226**, 347–366.

Donnelly, T. W. & Rogers, J. J. W. (1980). Igneous series in island arcs: the northeastern Caribbean compared with worldwide island-arc assemblages. *Bulletin of Volcanology* **43**, 347–382.

Donnelly, T. W., Beets, D., Carr, M. J., Jackson, T., Klaver, G., Lewis, J., Maury, R. C., Schellenkens, H., Smith, A. L., Wadge, G. & Westercamp, D. (1990). History and tectonic setting of Caribbean magmatism. In: Dengo, G. & Case, J. (eds) *The Geology of North America, Vol. H. The Caribbean Region*. Boulder, CO: Geological Society of America, pp. 339–374.

Draper, G., Gutiérrez, G. & Lewis, J. (1996). Thrust emplacement of the Hispaniola peridotite belt: Orogenic expression of the mid-Cretaceous Caribbean arc polarity reversal? *Geology* **24**, 1143–1146.

Dupuy, C., Liotard, J. M. & Dostal, J. (1992). Zr/Hf fractionation in intraplate basaltic rocks: carbonate metasomatism in the mantle source. *Geochimica et Cosmochimica Acta* **56**, 2417–2423.

Eggins, S. M., Woodhead, J. D., Kinsley, L. P. J., Mortimer, G. E., Sylvester, P., McCulloch, M. T., Hergt, J. M. & Handler, M. R. (1997). A simple method for the precise determination of >40 trace elements in geological samples by ICPMS using enriched isotope internal standardization. *Chemical Geology* **134**, 311–326.

Elliott, T. (2003). Tracers of the slab. In: Eiler, J. (ed.) Inside the subduction factory. *American Geophysical Union, Geophysical Monograph* **138**, 23–45.

Elliott, T., Plank, T., Zindler, A., White, W. & Bourdon, B. (1997). Element transport from slab to volcanic front at the Mariana arc. *Journal of Geophysical Research* **102**, 14991–15019.

Escuder Viruete, J., Díaz de Neira, A., Hernáiz Huerta, P. P., Monthel, J., García Senz, J., Joubert, M., Lopera, E., Ullrich, T., Friedman, R., Mortensen, J. & Pérez-Estaún, A. (2006). Magmatic relationships and ages of Caribbean Island arc tholeiites, boninites and related felsic rocks, Dominican Republic. *Lithos* **90**, 161–186.

Ewart, A. W. & Hawkesworth, C. J. (1987). Pleistocene to recent Tonga–Kermadec arc lavas: interpretation of new isotope and rare earth data in terms of a depleted mantle source model. *Journal of Petrology* **28**, 495–530.

Foley, S., Tiepolo, M. & Vannucci, R. (2002). Growth of early continental crust controlled by melting of amphibolite in subduction zones. *Nature* **417**, 837–840.

Forsythe, L. M., Nielsen, R. L. & Fisk, M. R. (1994). High-field strength element partitioning between pyroxene and basaltic to dacitic magmas. *Chemical Geology* **117**, 107–125.

García-Casco, A., Torres-Roldán, R. L., Iturralde-Vinent, M. A., Millán, G., Núñez-Cambra, K., Lázaro, C. & Rodríguez-Vega, A. (2006). High pressure metamorphism of ophiolites in Cuba. *Geologica Acta* **4**, 63–88.

Garrido, C. J., Bodinier, J. L. & Alard, O. (2000). Incompatible trace element partitioning and residence in anhydrous spinel peridotites and websterites from the Ronda orogenic peridotite. *Earth and Planetary Science Letters* **181**, 341–358.

Gómez-Tuena, A., Langmuir, C. H., Goldstein, S. L., Straub, S. M. & Ortega-Gutiérrez, F. (2007). Geochemical evidence for slab melting in the Trans-Mexican Volcanic Belt. *Journal of Petrology* **48**, 537–562.

Govindaraju, K. (1994). Compilation of working values and sample description for 383 geostandards. *Geostandards Newsletter* **18**, 1–158.

Green, T. H. (1995). Significance of Nb/Ta as an indicator of geochemical processes in the crust–mantle system. *Chemical Geology* **120**, 347–359.

Green, T. H., Sie, S. H., Ryan, C. G. & Cousens, D. R. (1989). Proton microprobe-determined partitioning of Nb, Ta, Zr, Sr and Y between garnet, clinopyroxene and basaltic magma at high pressure and temperature. *Chemical Geology* **74**, 201–216.

Gribble, R. F., Stern, R. J., Newman, S., Bloomer, S. H. & O'Hearn, T. (1998). Chemical and isotopic composition of lavas from the northern Mariana Trough: implications for magmagenesis in back-arc basins. *Journal of Petrology* **39**, 125–154.

Gyarmati, P., Méndez, I. & Lay, M. (1998). Caracterización de las rocas del arco de islas Cretácico en la Zona Estructuro-Facial Nipe–Cristal–Baracoa. In: Furrazola, G. F. & Nuñez-Cambra, K. E. (eds) *Estudios sobre Geología de Cuba*. Havana: Instituto de Geología y Paleontología, pp. 357–364.

Hart, S. R. (1984). A large-scale isotope anomaly in the Southern Hemisphere mantle. *Nature* **309**, 753–757.

Hawkesworth, C. J. (1982). Isotope characteristics of magmas erupted along destructive plate margins. In: Thorpe, R. S. (ed.) *Andesites: Orogenic Andesites and Related Rocks*. Chichester: Wiley, pp. 549–571.

Hawkesworth, C. J., Hergt, J. M., Ellam, R. M. & McDermott, F. (1991). Element fluxes associated with subduction related magmatism. *Philosophical Transactions of the Royal Society of London, Series A* **335**, 393–405.

Hawkesworth, C. J., Gallagher, K., Hergt, J. M. & McDermott, F. (1993). Mantle and slab contributions in arc magmas. *Annual Review of Earth and Planetary Sciences* **21**, 175–204.

Hochstaedter, A., Gill, J., Peters, R., Broughton, P. & Holden, P. (2001). Across-arc geochemical trends in the Izu–Bonin arc: Contributions from the subducting slab. *Geochemistry, Geophysics, Geosystems* **2**, article number 2000GC000105.

Hofmann, A. W. (2003). Sampling mantle heterogeneity through oceanic basalts: isotopes and trace elements. In: Carlson, R. W. (ed.) *Treatise on Geochemistry, The Mantle and Core, Vol. 2*. Amsterdam: Elsevier, pp. , pp. 61–101.

Iturralde-Vinent, M. A. (1996a). Geología de las ofiolítas de Cuba. In: Iturralde-Vinent, M. A. (ed.) *Ofiolítas y Arcos Volcánicos de Cuba. Caribbean Ophiolites and Volcanic Arcs. IUGS–UNESCO Project 364, Special Contribution*, pp. 83–120.

Iturralde-Vinent, M. A. (1996*b*). Cuba: el arco de islas volcánicas del Cretácico. In: Iturralde-Vinent, M. A. (ed.) *Ofiolítas y Arcos Volcánicos de Cuba. Caribbean Ophiolites and Volcanic Arcs. IUGS–UNESCO Project 364, Special Contribution*, pp. 179–189.

Iturralde-Vinent, M. A. (1998). Sinopsis de la Constitución Geológica de Cuba. In: Melgarejo, J. C. & Proenza, J. A. (eds) *Geología y Metalogenia de Cuba: una introducción. Acta Geologica Hispanica* **33**(1–4), 9–56.

Iturralde-Vinent, M. A., Díaz-Otero, C., Rodríguez-Vega, A. & Díaz-Martínez, R. (2006). Tectonic implications of paleontologic dating of Cretaceous–Danian sections of Eastern Cuba. *Geologica Acta* **4**, 89–102.

Jakeš, P. & Gill, J. (1970). Rare earth elements and the island arc tholeiitic series. *Earth and Planetary Science Letters* **9**, 17–28.

Johnson, D. M., Hooper, P. R. & Conrey, R. M. (1999). XRF analysis of rocks and minerals for major and trace elements on a single low dilution Li-tetraborate fused bead. *Advances in X-ray Analysis* **41**, 843–867.

Jolly, W. T., Lidiak, E. G., Dickin, A. P. & Wu, T. W. (2001). Secular geochemistry of central Puerto Rican island arc lavas: constraints on Mesozoic tectonism in the eastern Greater Antilles. *Journal of Petrology* **42**, 2197–2214.

Jolly, W. T., Lidiak, E. G. & Dickin, A. P. (2006). Cretaceous to Mid-Eocene pelagic sediment budget in Puerto Rico and the Virgin Islands (northeast Antilles Island arc). *Geologica Acta* **4**, 35–62.

Kalfoun, F. (2002). Géochimie du Niobium et du Tantale: distribution et fractionnement de ces deux éléments dans les différents réservoirs terrestres. *Mémoires des Géosciences de Montpellier* **27**, 275.

Kelemen, P. B., Hanghøj, K. & Greene, A. R. (2003). One view of the geochemistry of subduction-related magmatic arcs, with an emphasis on primitive andesite and lower crust. In: Rudnick, R. (ed.) *Treatise on Geochemistry, The Crust, Vol. 3.* Amsterdam: Elsevier, pp. 593–659.

Keppler, H. (1996). Constraints from partitioning experiments on the composition of subduction-zone fluids. *Nature* **380**, 237–240.

Kerr, A. C., Tarney, J., Marriner, G. F., Nivia, A. & Saunders, A. D. (1997). The Caribbean–Colombian Cretaceous igneous province: the internal anatomy of an oceanic plateau. In: Mahoney, J. J. & Coffin, M. (eds) *Large Igneous Provinces; Continental, Oceanic and Planetary Flood Volcanism. Geophysical Monograph, American Geophysical Union* **100**, 123–144.

Kerr, A. C., Iturralde-Vinent, M. A., Saunders, A. D., Babbs, T. L. & Tarney, J. (1999). A new plate tectonic model of the Caribbean: Implications from a geochemical reconnaissance of Cuban Mesozoic volcanic rocks. *Geological Society of America Bulletin* **111**, 1581–1599.

Kerr, A. C., White, R. V., Thompson, P. M. E., Tarney, J. & Saunders, A. D. (2003). No oceanic plateau—no Caribbean plate? The seminal role of an oceanic plateau in Caribbean plate evolution. In: Bartolini, C., Buffler, R. T. & Blickwede, J. (eds) *The Circum-Gulf of Mexico and the Caribbean: Hydrocarbon Habitats, Basin Formation, and Plate Tectonics, AAPG Memoirs* **79**, 126–168.

Kessel, R., Schmidt, M. W., Ulmer, P. & Pettke, T. (2005). Trace element signature of subduction zone fluids, melts and supercritical liquids at 120–180 km depth. *Nature* **437**, 724–727.

Klemme, S., Blundy, J. D. & Wood, B. J. (2002). Experimental constraints on major and trace element partitioning during partial melting of eclogite. *Geochimica et Cosmochimica Acta* **66**, 3109–3123.

Klemme, S., Prowatke, S., Hametner, K. & Günther, D. (2005). Partitioning of trace elements between rutile and silicate melts: Implications for subduction zones. *Geochimica et Cosmochimica Acta* **69**, 2361–2371.

Kogiso, T., Tatsumi, Y. & Nakano, S. (1997). Trace element transport during dehydration processes in the subducted oceanic crust. 1. Experiments and implications for the origin of ocean island basalts. *Earth and Planetary Science Letters* **148**, 193–205.

Lapierre, H., Dupuis, V., Mercier de Lépinay, B., Bosch, D., Monié, P., Tardy, M., Maury, R. C., Hernandez, J., Polvé, M., Yeghicheyan, D. & Cotten, J. (1999). Late Jurassic oceanic crust and Upper Cretaceous Caribbean Plateau picritic basalts exposed in the Duarte igneous complex, Hispaniola. *Journal of Geology* **107**, 193–207.

Lapierre, H., Bosch, D., Dupuis, V., Polvé, M., Maury, R. C., Hernandez, J., Monié, P., Yeghicheyan, D., Jaillard, E., Tardy, M., Mercier de Lépinay, B., Mamberti, M., Desmet, A., Keller, F. & Sénebier, F. (2000). Multiple plume events in the genesis of the peri-Caribbean Cretaceous oceanic plateau province. *Journal of Geophysical Research* **105**, 8403–8421.

Lebron, M. C. & Perfit, M. R. (1993). Stratigraphic and petrochemical data support subduction polarity reversal of the Cretaceous Caribbean island arc. *Journal of Geology* **101**, 389–396.

Lebron, M. C. & Perfit, M. R. (1994). Petrochemistry and tectonic significance of Cretaceous island-arc rocks, Cordillera Oriental, Dominican Republic. *Tectonophysics* **229**, 69–100.

Lewis, J. F. & Draper, G. (1990). Geology and tectonic evolution of the northern Caribbean margin. In: Dengo, G. & Case, J. (eds) *The Geology of North America, Vol. H. The Caribbean Region.* Boulder, CO: Geological Society of America, pp. 77–140.

Luais, B., Télouk, P. & Albarède, F. (1997). High-precision Nd isotopic measurements using plasma-source mass spectrometry. *Geochimica et Cosmochimica Acta* **61**, 4847–4854.

Mamberti, M., Lapierre, H., Bosch, D., Jaillard, E., Ethien, R., Hernandez, J. & Polvé, M. (2003). Accreted fragments of the Late Cretaceous Caribbean–Colombian Plateau in Ecuador. *Lithos* **66**, 173–199.

Marchesi, C., Garrido, C. J., Godard, M., Proenza, J. A., Gervilla, F. & Blanco-Moreno, J. (2006). Petrogenesis of highly depleted peridotites and gabbroic rocks from the Mayarí–Baracoa Ophiolitic Belt (eastern Cuba). *Contributions to Mineralogy and Petrology* **151**, 717–736.

McCulloch, M. T. & Gamble, A. J. (1991). Geochemical and geodynamical constraints on subduction zone magmatism. *Earth and Planetary Science Letters* **102**, 358–374.

Meschede, M. & Frisch, W. (1998). A plate tectonic model for the Mesozoic and Early Cenozoic history of the Caribbean plate. *Tectonophysics* **296**, 269–291.

Miyashiro, A. (1974). Volcanic rock series in island arcs and active continental margins. *American Journal of Science* **274**, 321–355.

Münker, C. (1998). Nb/Ta fractionation in a Cambrian arc/back arc system, New Zealand: source constraints and application of refined ICPMS techniques. *Chemical Geology* **144**, 23–45.

Münker, C., Pfänder, J. A., Weyer, S., Büchl, A., Kleine, T. & Mezger, K. (2003). Evolution of planetary cores and the Earth–Moon system from Nb/Ta systematics. *Science* **301**, 84–87.

Münker, C., Wörner, G., Yogodzinski, G. & Churikova, T. (2004). Behaviour of high field strength elements in subduction zones: constraints from Kamchatka–Aleutian arc lavas. *Earth and Planetary Science Letters* **224**, 275–293.

Murphy, J. B., Pisarevsky, S. A., Nance, R. D. & Keppie, J. D. (2004). Neoproterozoic–Early Paleozoic evolution of peri-Gondwanan terranes: implications for Laurentia–Gondwana connections. *International Journal of Earth Sciences* **93**, 659–682.

Nance, R. D. & Murphy, J. B. (1994). Contrasting basement isotopic signatures and the palinspastic restoration of

peripheral orogens: Example from the Neoproterozoic Avalonian–Cadomian belt. *Geology* **22**, 617–620.

Pearce, J. A. (1983). The role of sub-continental lithosphere in magma genesis at destructive plate margins. In: Hawkesworth, C. J. & Norris, M. J. (eds) *Continental Basalts and Mantle Xenoliths*. Nantwich: Shiva, pp. 230–249.

Pearce, J. A. & Parkinson, I. J. (1993). Trace element models for mantle melting: application to volcanic arc petrogenesis. In: Prichard, H. M., Alabaster, T., Harris, N. B. & Neary, C. R. (eds) *Magmatic Processes and Plate Tectonics. Geological Society, London, Special Publications* **76**, 373–403.

Pearce, J. A. & Peate, D. W. (1995). Tectonic implications of the composition of volcanic arc magmas. *Annual Review of Earth and Planetary Sciences* **23**, 251–285.

Pearce, J. A., Stern, R. J., Bloomer, S. H. & Fryer, P. (2005). Geochemical mapping of the Mariana arc–basin system: Implications for the nature and distribution of subduction components. *Geochemistry, Geophysics, Geosystems* **6**, article number Q07006.

Pin, C., Briot, D., Bassin, C. & Poitrasson, F. (1994). Concomitant extraction of Sr and Sm–Nd for isotopic analysis in silicate samples based on specific extraction chromatography. *Analytica Chimica Acta* **298**, 209–217.

Pindell, J. L. (1994). Evolution of the Gulf of Mexico and the Caribbean. In: Donovan, S. & Jackson, T. (eds) *Caribbean Geology, an Introduction*. Kingston: UWI Publishers′ Association, pp. 13–40.

Pindell, J. L. & Kennan, L. (2001). Kinematic evolution of the Gulf of Mexico and Caribbean. In: Fillon, R., Rosen, N., Weimer, P., Lowrie, A., Pettingill, H., Phair, R., Roberts, H. & van Hoorn, B. (eds) *GCSSEPM Foundation 21st Annual Bob F. Perkins Research Conference Transactions, Petroleum Systems of Deep-Water Basins*, Houston, TX: *GCSSEPM*. pp. 193–220.

Pindell, J. L., Kennan, L., Stanek, K. P., Maresch, W. V. & Draper, G. (2006). Foundations of Gulf of Mexico and Caribbean evolution: eight controversies resolved. *Geologica Acta* **4**, 303–341.

Plank, T. (2005). Constraints from thorium/lanthanum on sediment recycling at subduction zones and the evolution of the continents. *Journal of Petrology* **46**, 921–944.

Plank, T. & Langmuir, C. H. (1998). The chemical composition of subducting sediment and its consequences for the crust and mantle. *Chemical Geology* **145**, 325–394.

Plank, T. & White, W. M. (1995). Nb and Ta in arc and mid-ocean basalts. *EOS Transactions, American Geophysical Union* **76**(46), AGU Fall Meeting Supplement, 655.

Proenza, J. A., Díaz-Martínez, R., Iriondo, A., Marchesi, C., Melgarejo, J. C., Gervilla, F., Garrido, C. J., Rodríguez-Vega, A., Lozano-Santacruz, R. & Blanco-Moreno, J. (2006). Primitive Cretaceous island-arc volcanic rocks in eastern Cuba: the Téneme Formation. *Geologica Acta* **4**, 103–121.

Prouteau, G., Maury, R. C., Sajona, F. G., Cotten, J. & Joron, J. L. (2000). Behaviour of Nb, Ta and other HFSE in adakites and related lavas from the Philippines. *Island Arc* **9**, 487–498.

Quintas, F. (1988). Características estratigráficas y estructurales del complejo ofiolítico y eugeosinclinal de la Cuenca del Río Quibiján, Baracoa. *Revista Minería y Geología* **6**, 11–22.

Révillon, S., Hallot, E., Arndt, N. T., Chauvel, C. & Duncan, R. A. (2000). A complex history for the Caribbean Plateau: petrology, geochemistry, and geochronology of the Beata Ridge, South Hispaniola. *Journal of Geology* **108**, 641–661.

Ryerson, F. J. & Watson, E. B. (1987). Rutile saturation in magmas: implications for Ti–Nb–Ta depletion in island arc basalts. *Earth and Planetary Science Letters* **86**, 225–239.

Santos, J. F., Schärer, U., Gil Ibarguchi, J. I. & Girardeau, J. (2002). Genesis of pyroxenite-rich peridotite at Cabo Ortegal (NW Spain): geochemical and Pb–Sr–Nd isotope data. *Journal of Petrology* **43**, 17–43.

Schaule, B. K. & Patterson, C. C. (1981). Lead concentrations in the northeast Pacific: evidence for global anthropogenic perturbations. *Earth and Planetary Science Letters* **54**, 97–116.

Sinton, C. W., Duncan, R. A., Storey, M., Lewis, J. & Estrada, J. J. (1998). An oceanic flood basalt province within the Caribbean plate. *Earth and Planetary Science Letters* **155**, 221–235.

Sinton, J. M., Ford, L. L., Chappell, B. & McCulloch, M. T. (2003). Magma genesis and mantle heterogeneity in the Manus back-arc basin, Papua New Guinea. *Journal of Petrology* **44**, 159–195.

Stacey, J. S. & Kramers, J. D. (1975). Approximation of terrestrial lead isotopic evolution by a two-stage model. *Earth and Planetary Science Letters* **26**, 207–221.

Stolz, A. J., Jochum, K. P., Spettel, B. & Hofmann, A. W. (1996). Fluid- and melt-related enrichment in the subarc mantle; evidence from Nb/Ta variations in island-arc basalts. *Geology* **24**, 587–590.

Su, Y. & Langmuir, C. H. (2003). Global MORB chemistry compilation at the segment scale. Ph.D. thesis, Columbia University, New York.

Sun, S.-S. & McDonough, W. F. (1989). Chemical and isotopic systematics of oceanic basalts: implications for mantle composition and processes. In: Saunders, A. D. & Norry, M. J. (eds) *Magmatism in the Ocean Basins. Geological Society, London, Special Publications* **42**, 313–345.

Tatsumi, Y., Hamilton, D. L. & Nesbitt, R. W. (1986). Chemical characteristics of fluid phase released from a subducted lithosphere and origin of arc magmas—Evidence from high-pressure experiments and natural rocks. *Journal of Volcanology and Geothermal Research* **29**, 293–309.

Taylor, B. & Martinez, F. (2003). Back-arc basin basalt systematics. *Earth and Planetary Science Letters* **210**, 481–497.

Tiepolo, M., Vannucci, R., Oberti, R., Foley, S., Bottazzi, P. & Zanetti, A. (2000). Nb and Ta incorporation and fractionation in titanian pargasite and kaersutite: crystal-chemical constraints and implications for natural systems. *Earth and Planetary Science Letters* **176**, 185–201.

Todt, W., Cliff, R. A., Hanser, A. & Hofmann, A. W. (1996). Evaluation of a ^{202}Pb–^{205}Pb double spike for high-precision lead isotope analysis. In: Basu, A. & Hart, S. (eds) *Earth Processes: Reading the Isotopic Code. Geophysical Monograph, American Geophysical Union* **95**, 429–437.

Tohver, E., Bettencourt, J. S., Tosdal, R., Mezger, K., Leite, W. B. & Payolla, B. L. (2004). Terrane transfer during the Grenville orogeny: tracing the Amazonian ancestry of southern Appalachian basement through Pb and Nd isotopes. *Earth and Planetary Science Letters* **228**, 161–176.

Walter, M. J. (2003). Melt extraction and compositional variability in mantle lithosphere. In: Carlson, R. W. (ed.) *Treatise on Geochemistry, The Mantle and Core, Vol. 2.* Amsterdam: Elsevier, pp. 363–394.

Walter, M. J., Sisson, T. W. & Presnall, D. C. (1995). A mass proportion method for calculating melting reactions and application to melting of model upper mantle lherzolite. *Earth and Planetary Science Letters* **135**, 77–90.

Weaver, B. L., Wood, D. A., Tarney, J. A. & Joron, J. L. (1986). Role of subducted sediment in the genesis of ocean-island basalts: geochemical evidence from South Atlantic Islands. *Geology* **14**, 275–278.

White, M. W., Albarède, F. & Télouk, P. (2000). High precision analysis of Pb isotopic ratios by multi-collector ICP-MS. *Chemical Geology* **167**, 257–270.

Woodhead, J., Eggins, S. & Gamble, J. (1993). High field strength and transition element systematics in island arc and back-arc basin basalts: evidence for multi-phase melt extraction and a depleted mantle wedge. *Earth and Planetary Science Letters* **114**, 491–504.

Workman, R. K. & Hart, S. R. (2005). Major and trace element composition of the depleted MORB mantle (DMM). *Earth and Planetary Science Letters* **231**, 53–72.